OPTIMIZATION OF SYNTHESIS PARAMETERS OF TRANSITION METALS DEPOSITED ON CARBON STRUCTURES FOR ENHANCING ELECTROCATALYTIC ACTIVITY

by

Angela Macedo Andrade

A thesis submitted in partial satisfaction of
requirements for the degree of Master of Science

in

Mechanical Engineering

Committee in charge:
Professor Min Hwan Lee
Professor Lilian Davila
Professor Abel Chuang

The thesis of Angela Macedo Andrade is approved:

_____

Min Hwan Lee, Chair Date

_____

Lilian Davila Date

_____

Abel Chuang Date

To my family, for all their love and support.

ACKNOWLEDGEMENT

I wish to acknowledge my research advisor, Min Hwan Lee, for all his help, guidance, and encouragement. I would also like to thank my all my friends, mentors and colleagues for all their support, advice and love. I especially want to express my gratitude to Simranjit, Alireza and Ziqi for their invaluable assistance in conducting experiments.

TABLE OF CONTENTS

LIST OF FIGURES

LIST OF SYMBOLS AND ABBREVIATIONS

PEMFC	Polymer Electrolyte Membrane Fuel Cell
RFC	Regenerative Fuel Cell
GO	Graphene Oxide
TM	Transition Metal
ORR	Oxygen Reduction Reaction
OER	Oxygen Evolution Reaction
ALD	Atomic Layer Deposition
CV	Cyclic Voltammetry
LSV	Linear Sweep Voltammetry
RHE	Reversible Hydrogen Electrode
SEM	Scanning Electron Microscope
TEM	Transmission Electron Microscope
FTIR	Fourier Transform Infrared
TiO_2	Titanium Dioxide
G	Gibbs Free Energy

E	Potential Energy
j	Current Density
j_o	Exchange Current Density
F	Faraday Constant
η	Activation Loss
ω	Angular Frequency of Rotation

ABSTRACT

This study focuses on developing non-precious metal electrodes for oxygen reduction reactions (ORR) and oxygen evolution reactions (OER), the core catalyzes of fuel cells and electrolyzers, respectively. Specifically, metal oxides on carbon support are considered as the catalytically active electrode materials in this study. Two approaches of fabrication are presented: one based upon atomic layer deposition (ALD) and one by a wet synthesis process known as the solvothermal method. The resulting catalysts are characterized to reveal the process-performance relationship for ORR and OER.

The first study investigates the catalytic activities of titanium dioxide (TiO_2) incorporated onto graphene oxygen (GO) by atomic layer deposition (ALD). The catalytic activity was systematically measured by cyclic voltammetry (CV). Evidence shows that TiO_2 bonded on the surface of GO is catalytic active. Comparing the CV before and after ALD of TiO_2 shows improvement on the catalytic activity after deposition of TiO_2. Temperature effects, during deposition, were also measured by CV. The trends show that at higher temperature there is an increase in catalytic activity, which is due to the simultaneous reduction and addition of TiO_x during ALD. In addition, there is also an optimal amount of TiO_x that can be deposited for enhanced catalytic activity, which is 25 cycles.

In the second study, a bimetallic metal organic framework (MOF) was synthesized using cobalt and copper chloride, complexed with 2-aminoterephthalic acid and incorporated with graphene oxide (GO), which resulted in flower-like nanostructures. Effects of post-annealing on catalytic activity for this material were measured using CV

and linear sweep voltammetry (LSV). This bimetallic MOF material showed both ORR and OER activity in an alkaline environment. In addition, as the annealing temperature was increased to 700°C, the ORR and OER catalytic capabilities improved for this material resulting in an ORR half-way potential at around 0.72 V and OER on-set potential of 1.57 V (at 10 mA/cm^2). With the overall oxygen electrode performance gauged by the difference of ORR and OER metrics ($\Delta E = E_{OER,j=10} - E_{ORR,1/2} = 0.85$ V), the bimetallic MOF material has a potential of serving as an excellent bifunctional electrocatalyst for regenerative fuel cells.

CHAPTER 1. INTRODUCTION

Currently, over 80% of the energy consumed in the United States is produced from fossil fuels, which include coal, natural gas and petroleum.[1] Unfortunately, maintaining a high use of fossil fuel-based energy, with ever so growing world population, is predicted to upsurge issues already taking place including pollution, global warming, and pollution-related illness.

According to the U.S. Energy Information Administration, transportation is one of the biggest sectors for energy consumption. Transportation composes over 28% of the energy consumed by the U.S. in 2017. For this reason, one of the major focuses is finding a renewable energy source that can replace fossil fuel based internal combustion engines in the transportation sector. Presently, this creates a need for growth and expansion of electrified vehicles starting from automobiles and ranging to semi-trucks, marine vessels, aircrafts and space crafts.

In comparison to other sources of energy, hydrogen-based fuel cells and batteries are energy conversion devices that can produce electricity without forming harmful byproducts. In addition, fuel cells and batteries have a higher efficiency than commonly used internal combustion engines. According to the Department of Energy, while combustion engines have an efficiency of about 35%, hydrogen based fuel cells can reach an efficiency of up to 60% or even higher. The process in a combustion engine requires the conversion of chemical energy into heat energy that is then used for mechanical energy to create electrical energy. On the other hand, both fuel cells and batteries have the advantage

of producing electrical energy directly from chemical energy virtually emission free. This is a result of reduced number of moving parts in electrified vehicles.

However, in batteries, their reactants cannot be replenished continuously, and often the energy density of a battery is compromised by its scalability. Scaling batteries to large sizes is an issue because it is used as both for energy storage and as an energy conversion device. The more energy storage you need the bigger the size of the battery should be. The electrification by battery of big vehicles such as semi trucks, aircrafts and even spacecrafts becomes an issue. For NASA reducing fuel size is also a priority because pound per cost is an issue.[2] On the other hand, the scaling of a fuel cell is readily achievable because the reactant (or fuel) reservoir is separate from the actual energy conversion component.

For this reason, fuel cells have an advantage in achieving higher energy density (the amount of energy per given size or weight) than batteries. Batteries, on the other hand, have a higher power density (the rate of energy generation per given size or weight) due to faster redox reactions than fuel cells. The eventual goal of alternative energy conversion and storage devices is to compete against the conventional internal combustion engine (ICE), which has both high energy and power densities as seen in the Ragone plot (Figure 1).

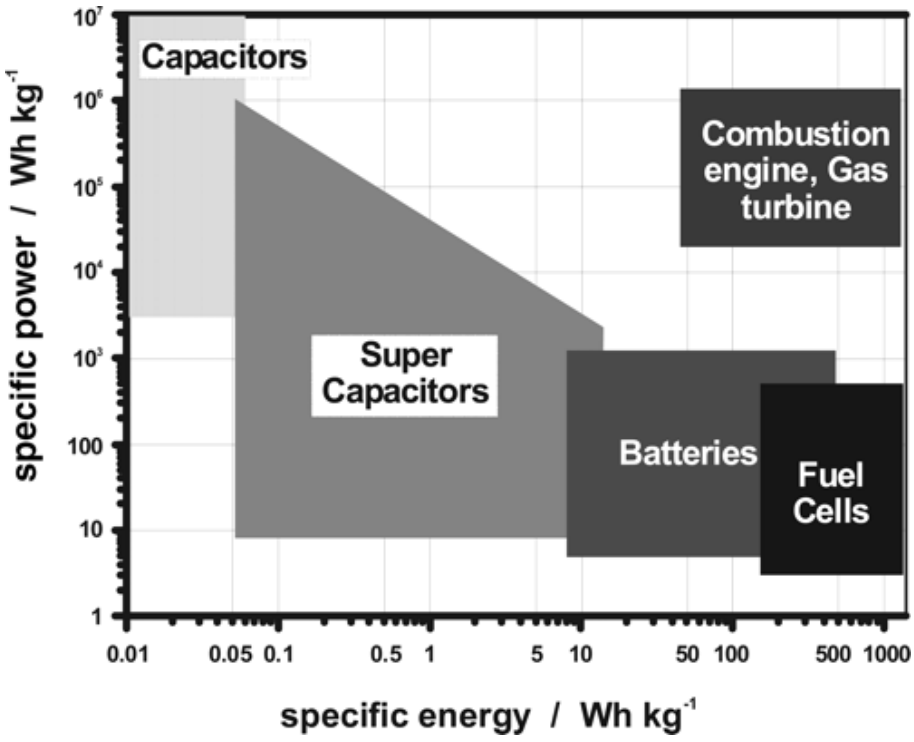

Figure 1. A simplified Ragone plot of the energy storage domains for the various electrochemical energy conversion systems compared to an internal combustion engine and turbines and conventional capacitors. (Adapted from M.Winter et al. [3])

Like in any other electrochemical energy devices, there are three main mechanisms of voltage loss that limit fuel cells form extracting all the thermodynamically determined voltage in an efficient way: redox reaction, ohmic transport and mass transport. The overpotential to incur a desired redox reaction is called activation loss. The activation loss, especially from ORR occurring at the cathode, is often the most detrimental losses in a hydrogen based fuel cell due to the sluggish kinetics of reducing oxygen into water. Comparatively, oxygen reduction is more than 6 orders of magnitude slower than hydrogen oxidation.[4] Thus, vast research and development for fuel cells including proton exchange membrane fuel cells (PEMFCs) has focused on the cathode material where ORR takes place.

Platinum has been readily used as an electrocatalytic material to mitigate the activation barrier against ORR. However, due to its prohibitive cost, scarcity and susceptibility to poisoning, there has been persistent research to find an alternative material. Most of the alternatives being developed are composed of non-precious metals, [5] heterogeneous material[6] or are completely metal free[7] that are mainly composed of carbon. Many of the newly developed alternative catalysts have been found not only more cost effective and abundant but also more efficient and durable than platinum.[8,9]

For fuel cells to be used as a self-sustained energy storage (in addition to an energy generator), they need to regenerate their reactants to continuously replenish and use them for energy production. A hydrogen-based cell equipped with both energy generation and recharging process is called regenerative fuel cells (RFCs). They not only function as a fuel cells, but operate as an electrolyzer for splitting water back into hydrogen and oxygen. In a RFC, this set-up provides a closed-loop system that is pollution free and can serve as a solution for not only the production of hydrogen, but of oxygen as well. In addition, the overall efficiency of a RFC is about 80% because is a closed system.[10]

To develop high-performance RFCs, an efficient catalyst not only for oxygen reduction but also oxygen evolution is necessary. Consequently, a key attribute for an electrocatalyst in RFCs would be bifunctionality in terms of oxygen electrode catalysis, i.e. ORR and OER.

Currently, there is a wide range of bifunctional catalysts from the well-known noble metal based such as Pt, Ir and Ru[11,12], transition metal compounds (TMCs) such as MnO_2[13] and Co_2O_3[14], metal sulfides like MoS_2[15], and metal-free bifunctional catalysts synthesized from doped carbon-based polymer nanostructure[16]. A commonly used bifunctional

electrocatalyst has been a noble metal mixture which includes platinum, ruthenium and/or iridium.[17] Again, these noble metal based materials are not desirable for use due to their high cost, and the negative affect they have on the environment. Bifunctional electrocatalyst made from transition metals, which is not only less expensive than noble metals but also made from a more abundant resource, have exhibited comparable performance to platinum in ORR and HER, and ruthenium and iridium in OER.[16,18,19]

Regardless whether the electrocatalytic reaction is ORR, OER or HER, these electrochemical reactions can be broken down into a series of simple steps that that include: 1. mass transport (reactant moves from bulk to near the electrode), 2. absorption (reactant approaches near the electrode), 3. chemisorbed (breaking of reactant bonds), 4. electron transfer (electrochemical charge transfer), and 5. desorption (product being released from electrode). For various electrocatalytic materials including noble metals, it is often not clear which of these processes is the rate limiting step responsible for high activation loss in a given condition. However, these processes do outline the attributes of good electrocatalysts such as high surface area, electronic conductivity, and electrochemical activity. Chemical and mechanical stability is additionally required.

The overall performance of an electrocatalyst is highly dependent on the morphological, structural and electronic configurations and composition of the catalyst material, which are affected by the condition of their synthesis process in terms of temperature, pressure, reaction time and reaction environment in addition to starting materials/precursors. Turning materials into nanostructures can also allow for higher performance per mass. Hybridization of dissimilar materials is another frequently employed approach; for example, incorporating transition metals into carbon structures

enhances the electrocatalytic activity further while providing them a support for potential nanoparticle that would otherwise aggregate.[20]

TMCs have the potential of forming different stoichiometry, which enables them to tune the absorption kinetics of oxygen and hydrogen and thus promote ORR, OER and HER. For some TMCs such as TiO_2 and Co_2O_3, a certain stoichiometry has shown to have better electrocatalytic performance for ORR[21,22], and others are good for water electrolysis.[5,17] The stoichiometry of TMCs can be altered by changing the environmental condition in terms of gas type, temperature and pressure. Another attribute of materials that affect their electrocatalytic performance is the crystal structure formed. Different crystal structures have distinct symmetries, atom arrangements, and bond structures. These can affect properties such as conductivity, chemical stability and mechanical stability, which can affect the efficiency of these electrochemical reactions. For instance, titanium oxide (TiO_x) is a polymorphous structure that has different types of tetragonal crystal structures[22,23]. Studies have shown that anatase structure has better catalytic activity than rutile structure, and even amorphous structure.[22]

As aforementioned, bifunctional catalysts are the key components of RFCs and metal-air batteries. Transition metal compounds supported on carbon structures have long been of high interest due to their low cost, abundance, facile synthesis, and have demonstrated to be able to catalyst both oxygen reduction reactions[24], oxygen evolution reactions[14], and hydrogen evolution reactions[25], which make them ideal candidates for their use in PEMFCs, RFCs and metal-air batteries. This thesis will present two approachess for synthesizing transition metals supported on carbon structures, using the so-called atomic layer deposition (ALD) and the solvothermal method, for their use as electrocatalysts in

PEMFCs and bifunctional electrocatalyst in RFCs. This paper will also present a parametric study to correlate the synthesis approach to electrocatalytic performance for ORR and OER.

CHAPTER 2. BACKGROUND

2.1 Overview of Polymer Electrolyte Membrane Fuel Cells

A fuel cell has three main components: two electrodes and an electrolyte (

Figure 2). Hydrogen-based PEMFCs have a polymer-based electrolyte that can provide high efficiency at low operating temperatures, around 80°C, with zero emissions and virtually silent operation. The polymer electrolyte membrane is usually made of hydrocarbons that contain fluorine groups and sulfonic groups to aid with the transfer of the ions and water while being highly resistant against electrons. The most commonly used polymer electrolyte membranes are Nafion (sulfonated tetrafluoroethylene based fluoropolymer-copolymer by DuPont) and persulfonated polytetrafluoroethylene (PTFE).

There are two electrochemical reactions occurring in hydrogen PEMFCs: hydrogen oxidation reaction (HOR) and oxygen reduction reactions (ORR). The oxidation of hydrogen in a PEMFC occurs in the anode side while the reduction of oxygen happens at the cathode side. These reactions produce electrical energy, heat and water. While the electrons produced from the oxidation of hydrogen at the anode side flow through an external circuit, which is used to power a device, the ions produced from this reaction flow through the polymer membrane electrolyte. The hydrogen ions along with the electrons head towards the cathode side to reduce oxygen into water. The electrochemical reactions occur in a location that is known as the triple phase boundary (TPB), where electrode material, electrolyte and incoming reactant meet altogether. As aforementioned, because

the kinetics of ORR is orders of magnitude slower than HOR, much of the focus for electrode design is focused on cathode side.[26]

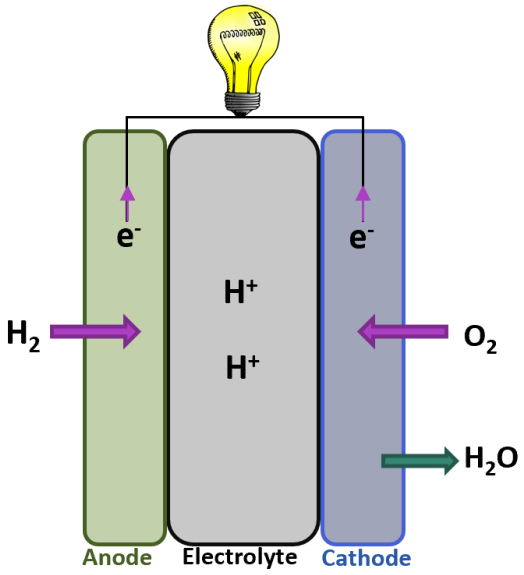

Figure 2. A simplified diagram of a PEMFC showing the basic three components: anode, cathode and electrolyte, and reactants and products

2.2 Overview of Regenerative Fuel Cells

Regenerative fuel cells (RFCs) have all the basic components of fuel cells but differ in that they can also operate as an electrolyzer (Figure 3b) for energy storage. An electrolyzer functions opposite to a fuel cell; instead of generating energy, it requires energy to split water into hydrogen and oxygen in what is known as hydrogen evolution reactions (HER) and oxygen evolution reactions (OER).

There are two main types of regenerative fuel cells. One type is known as a discrete regenerative fuel cells (DRFC) where the electrolyzer and fuel cell components are in two separate stacks. Unitized regenerative fuel cells (URFC), on the other hand, carry out the

electrolyzer and fuel cell functions in the same stack. For this reason, URFCs do not need an auxiliary heating because everything should happen in the same stack. It depends on the application to determine which type of regenerative fuel cell is a better option. URFCs can be a better choice when oxygen is stored and used, and DRFCs are a better choice when air is used for operating in fuel cell mode.[27]

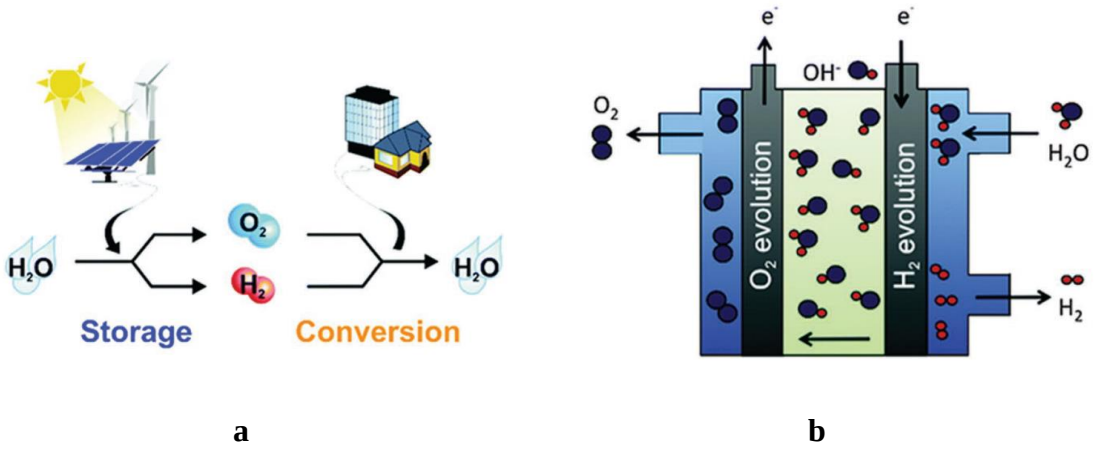

a **b**

Figure 3. a) hydrogen and oxygen cycles for energy storage and conversion. b) scheme of anion-exchange membrane electrolyzer (Adapted from D.Yan et al. [28])

The electrode design is also dependent on the type of regenerative fuel cell. For instance, the design of an electrolyzer cathode in a URFC, or where the evolution of oxygen occurs, is designed to allow for flooding. Flooding is when water covers the surface of the electrode material, which for an electrolyzer is needed to split water into oxygen. Whereas the fuel cell cathode, where oxidation reduction occurs, must repel water in order to prevent any blockage of active sites responsible for the electrocatalysis. Operation with pure oxygen in flooded or partially flooded electrodes may be feasible, particularly at elevated pressure.[10] Though for DRFCs, operation with air, has shown to have limitations in mass

transport. Even though RFC systems with different reactant combinations and electrolytes are possible, we will focus on hydrogen/oxygen systems using a proton exchange membrane electrolyte (PEM) in unitized regenerative fuel cell (URFC).

The electrode material in an URFC system not only has to catalyze ORR and HOR but should be able to split water to generate hydrogen and oxygen. Water electrolysis is usually defined by two reactions of hydrogen evolution reactions (HER) and oxygen evolution reactions (OER), and both require energy to occur. This means that the electrodes used in an URFC should either be a bifunctional or even trifunctional electrocatalysts. The goal for a bifunctional or trifunctional electrode material is for it to catalyze water splitting with minimal energy input, but it should still have the characteristics of a PEMFC electrode to catalyze HOR and ORR as well in an efficient way.

Setting up a new chapter

How do you begin a new chapter using this template? What must you do to get the page numbers to act correctly? Below are the steps for making a new chapter.

2.3 What is ORR, OER and HER (Thermodynamics of reactions)

In a PEMFC and RFCs, there are several electrochemical reactions involved. Depending on the catalyst and electrolyte environment, there are different products and intermediates for ORR, OER and HER. As previously mentioned, most of the electrochemical reactions involved in PEMFCs and RFCs occur at the triple phase boundary (TPB), and deal with the transfer of charge between electrode and chemical species.

The products formed by electrocatalysis of the reduction of oxygen depends on whether it happens in an acidic environment or basic environment. In general, ORR is a multi-electron reaction that can have different product formations. As seen in the equations below both acid and basic environment have a $4e^-$ and $2e^-$ process. For acid, the four-electron process produces water whereas in basic (or alkaline) environment the product is hydroxides.[29] In an alkaline medium, two different pathways of ORR (i.e. $4e^-$ or $2e^-$ process) can be described as:

$$O_2 + 2H_2O + 4e^- \rightarrow 4OH^- \quad (2.3.1)$$

$$O_2 + H_2O + 2e^- \rightarrow HO_2^- + OH^- \quad (2.3.2)$$

$$HO^-_2 + H_2O + 2e^- \rightarrow 3OH^- \quad (2.3.3)$$

The polymer electrolyte membrane is usually made from Nafion, and the fluorinated and sulfonic groups are made for an acidic environment. For this reason, PEMFC operation in an acidic environment is preferred. The ORR in acid can be written as:

$$O_2 + 4H^+ + 4e^- \rightarrow 2H_2O \quad (2.3.4)$$

$$O_2 + 2H^+ + 2e^- \rightarrow H_2O_2 \quad (2.3.5)$$

$$H_2O_2 + 2H^+ + 2e^- \rightarrow H_2O_2 \quad (2.3.6)$$

On the other hand, the reactions involved in OER and HER require external energy input and have a different set of reactants (as shown in the equation below).

$$2H_2O + \text{Energy} \rightarrow 2H_2 + O_2 \quad (2.3.7)$$

Again, the products of these reactions depend on the environment they take place as seen below, which result in different intermediates and products.[30]

In alkaline media

$$4H_2O \rightarrow O_2 + 2H_2O + 4e^- \quad (2.3.8)$$

$$4H_2O + 4e^- \rightarrow 2H_2 + 4OH^- \quad (2.3.9)$$

In acid media

$$2H_2O \rightarrow O_2 + 4H^+ + 4e^- \quad (2.3.10)$$

$$4H^+ + 4e^- \rightarrow 2H_2 \quad (2.3.11)$$

Regardless of the specifics of each reaction, most of these electrochemical reactions occurring in both PEMFCs and RFCs can be broken down into a series of steps, which include: mass transport, absorption, separation (O_2 molecules chemisorbed on the electrode surface), electron transport and mass transport.

A spontaneous chemical reaction renders a certain amount of energy available to do work, which is quantified by the Gibbs free energy of reaction. Even though this energy can be converted into different forms, for fuel cells the main focus is to try to convert as much of the chemical potential to electrical work. The Nernst equation (Equation 2.4.1 expounds just that, showing that Gibbs free energy ($\Delta\hat{g}$) sets the magnitude of the electrical potential (E) for an electrochemical reaction. In this equation, n is the number of moles of electrons transferred and F is Faraday constant. At standard conditions, the reaction, H_2 + ½O_2 → H_2O, produces 1.229 V by the following equation.

$$\Delta\hat{g} = -nFE \quad (2.4.1)$$

For electrochemical reactions that occur at a non-standard condition, the Nernst Equation can be used to quantify the reversible voltage. In fact, PEMFCs are usually operated at a non-standard condition (~ 80°C). The equation describes how the reversible voltage potential (E) varies with temperature and reactant/product activities.

$$E = E^0 - \frac{RT}{nF} \ln \frac{a_{Products}}{a_{Reactants}} \quad (2.4.2)$$

E^0 refers to the reversible cell potential at the standard condition, R is the gas constant, T is temperature and a is the activity of corresponding species involved in the electrochemical reaction. This depends on the chemical nature it takes on, and it could be for an ideal gas, nonideal gas, dilute ideal solution, nonideal solutions, pure components or metals. The reversible cell potential indicates the maximum electrical potential that could be extracted from an electrochemical reaction at a given temperature and reactant activity, and tells you the minimum amount of voltage input for that reactions to go in reverse. It could also be considered as the chemical potential difference between reactants and products.

2.4 A Brief Overview of the Kinetics of Electrochemical Reactions

The kinetics of electrochemical reactions, on the other hand, determine how fast and efficient these reactions proceed. Usually, the rate of a reaction is limited by the energy levels of its intermediate step(s). The energy path required to form a final product or reactant requires to overcome free energy differences between intermediates. This energy to be overcome is called an energy barrier. The rate of conversion of reactants to products

(or vice versa) depends on the probability of that reactant species being at an activated state, which is the state that is capable of transitioning to either products or reactants.

The probability of finding a species in the activated state is denoted as P_{act} in the following equation. As shown P_{act} is exponentially dependent on the activation energy (ΔG^*), which is the size of the activation barrier. The probability of finding an active state species can be used as a direct way to measure the rate of these reactions.

$$P_{act} = e^{-\Delta G^*/RT} \quad (2.4.3)$$

Regardless of the whether products or reactants are being formed, electrons are either being generated or consumed by these electrochemical reactions. This exchange of electrons is captured as current (i), which is the rate of charge over time. The current generated is proportional to the area of the triple phase boundary, or the active surface area where these reactions occurs. If the active surface area is increased, the rate of the reaction should increase as well. Current normalized by the active surface area (A) is known as current density (j). With this parameter, the reactivity of different catalyst in a given catalysis can be compared per unit area.

$$j = \frac{i}{A} \quad (2.4.4)$$

The current density is often used to describe the overall net reaction rate, which can be denoted as the rate of forward reaction (j_1) minus the rate of the reverse reaction (j_2). When these two reactions reach an equilibrium, that is when $j_1 = j_2 = j_0$, the net reaction rate is zero. This indicates that both the forward and reverse reactions are taking place at the same rate, where j_0 is known as the exchange current density.

Often, the forward reaction rate is likely to proceed faster than the reverse reaction rate in a spontaneous reaction. However, the unequal rates quickly result in a buildup of charge over time, which results in a potential difference (known as the Galvani potential) that counterbalances the free energy difference between the reactant and product states. This establishes an electrochemical equilibrium with a net reaction current equal to zero.

In order to produce a net current from a fuel cell, the Galvani potentials at the anode and the cathode should be reduced such that the forward reaction is favored. This is done by sacrificing part of the cell voltage. The voltage being sacrificed is also known as the overpotential or voltage loss. The Butler-Volmer (B-V) equation describes how much of the cell voltage needs to be sacrificed for a given reaction at a given temperature.

In addition, the B-V equation shows the current density (j) extracted from a cell has an exponential relationship with the overpotential (η).

$$j = j_0(e^{\alpha nF\eta/(RT)} - e^{-(1-\alpha)nF\eta/(RT)}) \quad (2.4.5)$$

where α is the transfer coefficient, which depends on the symmetry of the activation barrier. The B-V equation could be simplified given certain conditions. A linear approximation can be used when the activation loss (η) is small. The linear approximation comes from a Taylor series expansion and ignoring exponential with powers higher than 1.

$$j = j_0 \frac{nF\eta}{RT} \quad (2.4.6)$$

Another simplification done to the B-V equation is the Tafel approximation, which is used at large η (usually when $j > j_0$). In this case, the forward reaction dominates, and the reverse component disappears resulting in the following equation:

$$j = j_0 e^{\alpha nF\eta/(RT)} \quad (2.4.7)$$

Overall, improving the kinetics of the electrochemical reactions in a cell involves increasing j_0. Recall that j_0 is the exchange current density of the forward and reverse reaction at equilibrium, which is affected by various parameters including temperature, activation energy, reactant concentration and surface area. This set of equations help with identifying what characteristics of a material affect the kinetics and overall performance of a fuel cell, which aids in the design of an effective electrocatalyst.

2.5 Precious-metal based Electrode Material

Noble metals such as: platinum (Pt), iridium (Ir) and ruthenium (Ru) can catalyze ORR, OER and HER to have faster reaction kinetics that are good for commercialization of fuel cells.[31,28] Platinum is well known for catalyzing oxygen reduction reactions (ORR) and hydrogen evolution reaction (HER), especially in an acidic environment. The electrocatalytic mechanism of Pt for ORR in an acidic media involves a four-electron process.

The efficiency of the precious metal electrode materials is due to their d-band vacancies and shorter metal to metal interatomic distances that allow for strong metal-reactant interactions during the separation state (also known as dissociative adsorption) of ORR, OER and HER.[29] The separation state is often described as the chemisorption of the reactants to the surface of the electrode material. Considering ORR as an example, the interaction between Pt and oxygen during the separation state weakens the oxygen-oxygen bonding and therefore promotes the dissociation of oxygen molecules into water.[32] Chemisorption is referred to the adsorption of reactants to the surface of the electrode that involves a chemical reaction.

In contrast to ORR, electrocatalysis of hydrogen evolution reactions (HER) and oxygen evolution reactions (OER) requires energy input. Like ORR, platinum is still one of the materials that catalyze HER most efficiently (Figure 4).

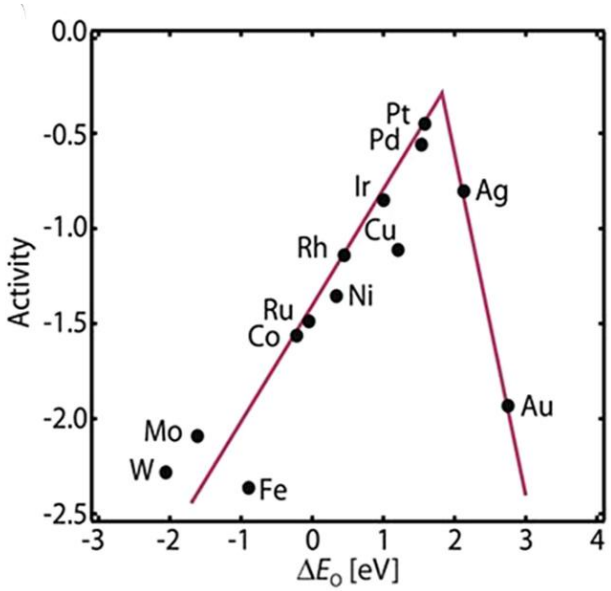

Figure 4. Volcano plot for oxygen reduction reaction (ORR) (Adapted from Z.W.Seh et al [33].

Theoretical calculations concluded that the overall reaction rate of HER was highly dependent on the Gibbs free energy of hydrogen adsorption (ΔG_H). Pt is an excellent catalyst with a ΔG_H close to zero, which indicates that the binding energy between Pt and hydrogen is not too weak or too strong.[34]

Ruthenium (Ru) and iridium (Ir) on the other hand, are well known OER electrocatalyst (as seen in Figure 2.4). Like Pt, Ru and Ir aid in the absorption and chemisorption of the reactants and intermediates in OER. Despite the difference among

these electrochemical reactions, most of the reactions occur via several steps that has a distinct rate-determining step intermediate.

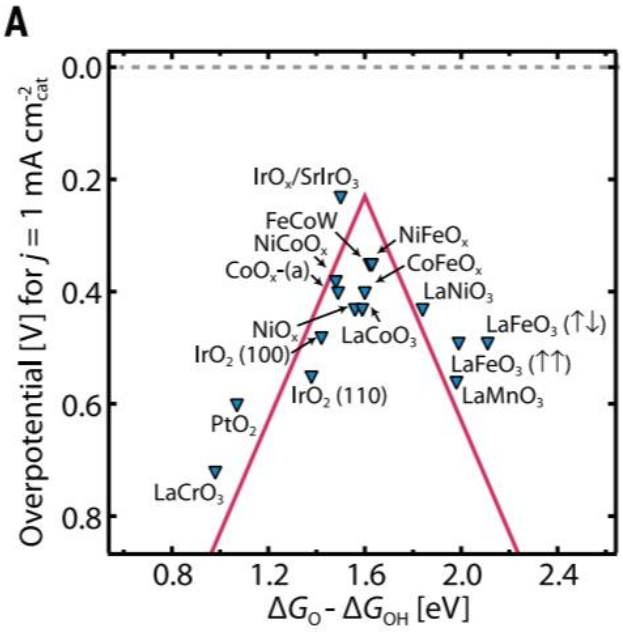

Figure 5. Volcano plot for oxygen evolution reaction (OER) (Adapted from Z.W.Seh et al [33].

2.6 Issues with Noble Metals

As discussed, despite, there are many issues that come with the use of precious metals as a catalyst, despite their excellent catalytic activity toward ORR, OER and HER. These include cost, resource scarcity and poisoning issues. An approach of mitigating this issue has been using less platinum by making nanostructures that will still render an efficient electrocatalysis. Some of these nanostructures including jagged Pt nanowires rendered record-breaking specific mass activity and electrochemical surface area.[35] Another way is creating alloys with other inexpensive metals, which still maintains a high electrocatalytic efficiency.[36] However, noble metals, especially Pt, show reduced

efficiency for catalyzing ORR over long-term cycling. In particular, in the presence of carbon dioxide (CO_2) and carbon monoxide (CO), Pt loses most of its catalytic activity towards oxygen.[16]

2.7 Non-precious Metal Electrocatalyst

With the many issues with noble metals as an electrocatalyst, there have been decades of investigations to find alternative materials that could avoid these issues. These materials range from metal free carbon structures to transition metal complexes[31,5,37], and other heterogeneous material (usually a hybrid between metal and non-metal structures).[38,39] What is sought out for in these materials is their easy synthesis, abundant nature, and their ability to perform the same electrocatalytic function as the noble metals. As previously discussed, most of the electrochemical reactions in fuel cells occur on the surface of electrode and electrolyte interface. For this reason, the surface properties of the electrode material are a key component for synthesizing stable and highly active electrocatalyst.

Research over the last several decades has shown that surface defects in electrode materials could be beneficial for enhancing electrocatalytic performance, and potentially could be more active than pristine defect-free material. Defects can provide an opportunity to enhance catalytic by modifying electronic properties as is the case of heteroatomic doped carbon material.[40,41] Other defects include cation and anion defects in transition metal structures that can aid in enhancing ORR, OER and HER.[42,43,44]

2.8 Metal-free Carbon Electrode Material

Graphene and its derivatives have been highly investigated for their material properties that are advantageous for a wide range of applications. In many electrocatalytic materials, carbon structures such as graphene and carbon nanotubes have played the role of being supportive structures providing a physical surface for dispersing small metal particles or nanostructures.[45,46] However, in recent years, metal free electrocatalyst have also shown to have exceptional electrocatalytic abilities.[31,16]

Defects in a graphene-based material itself can improve electrocatalytic properties. Defects induced by heteroatomic doping can aid in the redistribution of electronic energy profile, which has been shown to change the chemisorption mode of reactants such O_2 in ORR by waken the O-O bonding.[39,28] A doping often induces defects while the overall crystal structure is unchanged. Heteroatoms, such nitrogen, can alter the electronic properties of the nearby carbon atoms due to differences in atomic size, electronegativity and other factors.[41] Nitrogen, sulfu and phosphorus are all commonly used dopants in carbon-based materials, which can serve as a base structure material to enhance the electrocatalytic properties of transitional metal and transitional metal structures.[47,48,49]

In some cases, heteroatoms like nitrogen can be removed to form vacancies. Yao et al. prepared a 2D graphene material with carbon defects (DG) by a facile heat treatment process.[50] This process created many types of single-atom vacancies induced by N-atom removal. Data confirmed the absence of nitrogen in the material, which resulted in various defects on the edge of graphene at the atomic scale, including pentagons, heptagons and octagon. These defects modulated the local electronic environment and perturbed the surface properties of the graphene, such as the specific surface area and hydrophobicity. Authors showed that DG has higher catalytic active than original graphene sample and

studied the role of these defects for different electrochemical reactions, including ORR, OER and HER.

2.9 Transitional Metal Electrocatalyst

Even though the electrocatalytic mechanisms for transitional metals are still ambiguous, there are some characteristics attributed to improving their overall electrocatalytic performance. One of the key advantages of transitional metals is that they can take up different oxidation states, which has shown to alter their catalytic performance, and allow for bifunctional electrocatlaysis.[51,22,52] Some of the approaches to change their oxidation states is by heat treatments, plasma treatment, their composites with carbon supports, and creating defects that result in electrode material that can catalyze ORR and OER.[53,43]

The main defect in transitional metal oxides (TMOs) is oxygen vacancy. Its concentration and distribution can adjust the bandgap or charge distribution of the materials. The presence of vacancies is known to improve the kinetics of adsorbing reactants because the electronic energy profile can be tailored by changing the concentration of oxygen defects. For instance, a study done on cobalt oxide nanowires (NWs) showed that a reduced form of Co_3O_4 in NWs outperformed pristine Co_3O_4 in OER catalysis.[54] Experimental data and density functional theory (DFT) calculations showed that with the formation of oxygen vacancies in the reduced form of Co_3O_4, the two electrons that previously occupied the oxygen 2p orbitals became delocalized around the adjacent

three Co^{3+} and O atoms. In comparison to pristine Co_3O_4, the defect-rich Co_3O_4 resulted in an improved OER performance.

In addition to anion vacancies, cation vacancies can also influence the electrocatalytic performance of transitional metal (TM) material. This is especially true for transitional bimetallic material, and researchers have developed a variety of methods to prepare metal-cation vacancies. An example is the Mn-Co defect rich spinel structure that has high performance in both ORR and OER.[55] For this work, one of rate limiting steps in ORR and OER is the adsorption of oxygen. The results indicated that cobalt or manganese defect sites have different oxygen-binding abilities due to the mix metal valency, which affect the overall ORR and OER performance.

2.10 Metal Organic Frameworks

In addition to being doped with other materials, TMs can be complexed with organic linkers to form what are known as metal organic frameworks (MOFs). MOFs are orderly structured material with high surface area, and contain uniform open pores that can expose active metal sites. In the past few years, MOFs have garnered attention for their electrocatalytic abilities. MOFs can also benefit from defects for high electrocatalytic performance.

Like previously mentioned for bimetallic materials, MOFs have the advantage of having mixed valency between the two metals because they can tune the electrocatalytic activity by creating defects. Similarly, bimetallic MOFs have the same advantage, and it has been shown that a mixture of different metals can result in unsaturated coordinated

sites that are beneficial for OER catalysis. An example would be Co-Ni ultrathin nanosheets that are composed of MOFs. Nickel and cobalt metals are complexed with benzene dicarboxylic acid (BDC) organic linker.[56] The resulted MOF material had crystal defects with unsaturated metal sites on the surface and partially terminated BDC coordination bonding. Such coordinated unsaturated metal sites are active metal sites, which resulted in exceptional OER performance with a very low overpotential.

CHAPTER 3. OVERIEW OF MATERIAL SYNTHESIS AND CHARACTERIZATION

3.1 Material Synthesis

Both morphological properties (including shape, surface area, and dispersion of active materials) and chemical properties (type and concentration of defects, interfacial nature, etc.) of a catalyst are critical factors of overall catalytic performance of the material.[57,58] Crystalline nanostructures are often used as electrocatalytic material because their organized structure can provide enhanced electric conductivity and optimized dispersion of catalytically active sites, and allow for easier characterization of material structure (compared to amorphous structures) facilitating further optimization of the material for performance.[59,60] For most synthesis methods, both solution-based and vapor transport-based ones, the molecular and crystal structure in a material is often dictated by the process of nucleation and growth. Controlling these processes can lead to an electrocatalytic material with desired physical properties for fuel cell applications.

Nanostructure synthesis ultimately depends on the modes of nucleation (homogenous vs heterogeneous), the rate of nucleation (determined by the kinetics and thermodynamics of a reaction), the physical state of reactants or precursors (liquid, vapor, solution) and role of defects. Homogeneous nucleation is mostly hard to achieve because it requires a simultaneous nucleation throughout the surface (or interface). Therefore,

heterogeneous nucleation occurs in most cases. It starts by forming a wall of transformed material and then nucleates towards the inside of those walls regardless of the nucleation type (e.g. liquid-to-solid transformation, a transformation into a different solid phase, etc.).

Generally, the thermodynamics of forming certain material during nucleation depends on a range of parameters as seen in the equation below.[61]

$$\Delta g = -\left\{\frac{[(4/3)\pi r^3]}{\Omega}\right\} + 4\pi r^2 \alpha \text{ (homogeneous nucleation)} \quad (3.1.1)$$

$$\text{where } r = 2\Omega\alpha / kT\sigma$$

$$\Delta g_n = (16/3)\pi\alpha^3(\Omega/k_B T\sigma)^2 \text{ (heterogeneous nucleation)} \quad (3.1.2)$$

where Δg_n represents the Gibbs free energy of nucleation, α is the interfacial free energy, Ω volume per molecules, k_B is Boltzmann constant, r is the critical radius and T is temperature. These simplified equations reveal the critical parameters needed to synthesize a material with specific nanostructure and morphology. One of the focus of synthesizing electrode material is to create nanostructure material with defects, morphology and crystallinity that will promote the adsorption, chemisorption and separation of reactants involved in ORR, OER and HER.

3.2 Overview of Solvothermal Method

The solvothermal method involves dissolving a set of precursor or reactants in a solvent, and then having the resulting solution undergo a heat treatment in a pressurized autoclave. This environment enables crystallization, particle/crystal growth, and change in pore size volume. The solvothermal method process is used to make single crystals, nanocrystals and thin films.[62,] It is often used because of the simplicity and its capability

to prepare thermodynamically stable and metastable states of a material (or a composite) that would be difficult to form with other methods.

The overall material synthesis using the solvothermal method is controlled by different parameters including: solvent, precursor concentration, kinetics of crystal formation, temperature, pressure, etc. Materials such as metal organic frameworks, zeolites, metal/oxide nanoparticles, and other hybrid materials are synthesized using this method.[63,64,65] In general, solvothermal method is a facile, scalable and cost effective approach of synthesizing hybrid materials for many applications including catalysts.

3.3 Overview of Atomic Layer Deposition

Atomic layer deposition (ALD) is a type of vapor deposition that can has unique advantages over the other vapor deposition methods. While others vapor deposition methods run on a continuous flow of precursor, substrates in an ALD process is exposed to a sequence of precursor pulses. After a precursor gas is fed into the reaction chamber, adsorbed on the substrate and reacted with the substrate surface, all the unreacted precursor and products generated by the reaction will be purged away by an inert gas flow. The precursors used in ALD are designed to only react with the specific sites on a substrate's surface, and not react with each other. Therefore, the reaction is self-limiting, and a deposition beyond a single atomic layer per cycle is prohibited in a true ALD mode. After the first reaction followed by purging process, a second set of precursor gas will be introduced to the chamber and react with the substrate surface. This digitized process, as opposed to a continuous introduction of reactant, enables a highly accurate thickness control down to atomic scale, even on a substrate with highly complicated geometry.

Commonly used precursors in ALD are organometallic based compounds that help promote self-limiting surface reactions. The overall composition and structure of the substrate used for ALD affect the resulting deposition.

ALD has been used in a range of applications including batteries, fuel cells, photovoltaics, catalysis, semiconductors, and other electronics devices. ALD can aid in functionalization of material surfaces by forming ultrathin film or nanoparticles with size control down to the atomic scale. Since electrocatalysis is a highly surface-sensitive process, the ALD-based approach should provide ample opportunities for catalyst development.

As briefed, ALD growth is a multi-step process as follows: [66]

1. The substrate inside the chamber is exposed to a gaseous metal precursor for a certain amount of time. The reaction of a metal precursor with the substrate is referred as the first half reaction, where the ligands of the metal precursor are partially removed by reacting with the active sites on the substrate surface.[67] Then when the first half reaction is completed, the pulsing of the precursor is stopped. If the pulse time is enough for deposition, the molecules of the precursor will be allowed to react with all the sites on the substrate's surface, and one atomic layer of precursor molecules will be covering the surface.

2. The chamber is purged using an inert gas such as nitrogen and argon to remove any unreacted material.

3. Then there is the introduction of a second precursor into the chamber, which is to prepare another of reactive group layer for the first precursor to react. Pulsing of

the oxidant precursor is considered as the second half reaction that deposits oxides to the substrate surface. Usually, oxygen functional groups such as hydroxyls react well with ligand and metal center in a precursor, which allows the metal site to bind to the substrate surface.[68]

4. Step 2 is repeated using the same inert gas.

Steps 1-4 is considered as one full cycle. In an ideal case, the number of ALD cycle should be linearly proportional to the resulting thickness of the film. However, the deposition rate (i.e. thickness per full cycle) varies depending the precursor, substrate material and temperature.

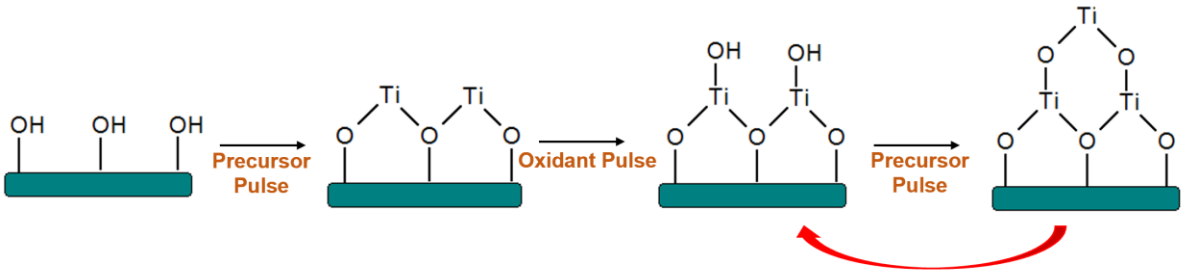

Figure 6 A schematic diagram depicting the ALD process of depositing titanium oxide on a hydroxylated substrate.

3.4 Material Characterization

Material characterization can be divided into two parts. One of the material characterizations is focused on characterizing the material composition and structure, while the other focuses on the electrochemical characterization to understand the process-property-performance correlation.

3.5 Scanning Electron Microscopy (SEM)

Scanning electron microscopy (SEM) uses a focused electron beam to scan over the surface of a material, which gives off various signals after interacting with atomic in the sample. A detector reads the signals and construct the surface topography of the material based upon them. The SEMs used in this study is a field emission gun-SEM (Zeiss Gemini 500 FEG-SEM) and an environmental SEM (FEI XL30). Both SEMs have various detectors including in-lens detector, secondary detector and backscatter detector. The latter is equipped with energy dispersive spectroscopy (EDS), which is used to characterize the elemental characterization of a material using the X-rays given off by the material. Each element in a sample has a distinctive energy difference between the outer and inner electron shells, which allow for elemental identification.

3.6 Fourier Transform Infrared (FTIR)

Fourier-transform infrared (FTIR) spectroscopy measures the infrared spectrum of transmittance or absorbance of a sample that is exposed to a wide range of wavelengths of infrared radiation. Some of the IR radiation is absorbed by the sample while some passes through. The energy absorbed or transmitted by the sample is related to the different vibrations of chemical bonds which include stretching and bending. By measuring the wavenumbers of the energy absorbed by a particular sample, chemical bondings within the sample are identified.[69] Unlike dispersive spectroscopy where a monochromatic beam is used, FTIR collects signals with a wide range of wavelengths simultaneously and process the raw data by leveraging Fourier transform.

3.7 Electrochemical Measurements

For this study, an electrochemical analyzer (Biologic SP-200; apotentiostat/galvanostat and impedance spectroscopy) is mainly used to perform cyclic voltammetry (CV), linear sweep voltammetry (LSV) and electrochemical impedance spectroscopy (EIS). A rotating disk electrode (RDE) apparatus (ALS RDE-3A) was used to obtain LSV at different rotational speeds. For all electrochemical measurements, a three electrode set-up was used to gauge ORR and OER capabilities of synthesized materials. In the three-electrode set-up, a 0.3 mm glassy carbon electrode (GCE) was deposited with sample, which served as the working electrode. A platinum wire (and graphite rod) was used as a counter electrode and silver-silver chloride (Ag/AgCl) in saturated potassium chloride was used as the reference electrode.

Cyclic voltammetry (CV) is a potential-sweeping technique that measures the resulting current from the cell of test. The potential is applied at a specific rate within a desired potential window and cycling back in the same potential window. A potential sweep towards higher anodic potentials gives rise to an oxidation current, while reduction occurs as the potential is being cycled back towards the cathodic potential. CV usually provides an initial assessment about the relative amplitude of electrochemically active surface area, presence of specific redox reactions and their relative activity.

Linear sweep voltammetry (LSV) is commonly used with a RDE to measure kinetic information of the catalytic capabilities of materials. Using a RDE allows for the extraction of the Tafel slope, an indication of catalytic activity.[70] The RDE allows for the convective flow of reactant to the surface of the working electrode thus creating a steady-state

diffusion where the mass transport dependent current, i_l, can be described with the following Levich equation:

$$\mathrm{i_l} = \mathrm{nFAD}^{2/3}\omega^{1/2}\nu^{-1/6}\mathrm{C}^{*} \quad (3.7.1)$$

where n is the number electron moles, F is Faraday's constant, D is the diffusion coefficient of the reactant, C^* bulk concentration of the reactants, ν is the kinematic viscosity of the solution, ω is the angular frequency of rotation, and A surface area.

This equation can then be combined with i_k, which is the kinetically dependent current which results in the Kourtecky-Levich equation that describes the current from electrochemical reaction dependent on kinetics and mass-transport:

$$\frac{1}{\mathrm{i}} = \frac{1}{\mathrm{i_k}} + \frac{1}{\mathrm{i_l}} \quad (3.7.2)$$

Often the constants terms ($nFADvC^*D$) of i_l are combined in one term, B, known as the Levich slope. This value can be obtained by plotting the reciprocal current of the sample versus the reciprocal of the rotational frequency. From the Levich slope, the number of electron moles can be calculated by dividing the slope by all the constants except for n, which is what we are solving for.

CHAPTER 4. TIO_2 OXIDE FUNCTIONALIZATION ON GRAPHENE OXIDE BY ATOMIC LAYER DEPOSITION

4.1 Introduction

Titanium dioxide (TiO_2) is an abundant, inexpensive and non-toxic material that has been widely used for a variety of applications ranging from sunscreens, solar cells, optics to photocatalyzers.[71] TiO_2 versatility is due to its tunable properties that can enhance its electrocatalytic performance[72] by modifying its chemical and physical properties.[73] The catalytic activity of TiO_2 can also be significantly enhanced by incorporating them onto an electron-conducting scaffold made of nanostructured carbon such as reduced graphene oxide (rGO).

Graphene oxide (GO) can be chemically reduced to graphene-like materials with excellent mechanical and chemical properties, and work as a useful precursor for the synthesis of functionalized graphene, which potentially renders a unique mechanical, electrochemical and electronic properties.[74] Since GO itself has very low electron conductivity, it needs to be reduced for use as an electrode material. As an approach of reducing GO, TiO_2 can be used; from UV-irradiated TiO_2 suspensions, GO accepts electrons and thus becomes reduced.[75] The TiO_2 tethered on the GO is also found to prevent restacking of graphene sheets, which is advantageous to use the resulting hybrid as a

catalyst. The rGO incorporated with TiO_2 is a commonly used material as photocatalyzers,[76] but it was rarely considered for ORR catalysis.

Recent studies have shown that the TiO_2 can have catalytic activity towards ORR. It was observed that ordered phases of TiO_2 crystals can facilitate electron transport, which enhances its catalytic activity towards the reduction of oxygen.[77] Titanium oxide is a polymorphous structure that has three common phases: anatase, rutile and brookite.[23] This study not only showed anatase as the optimal phase for ORR catalysis, but also showed that the oxygen vacancies in sub-stoichiometric TiO_{2-x} provides favorable site for oxygen binding, and thus facilitating its reduction. Forming oxygen vacancies, or reducing TiO_2, can be done in several ways such as doping [78], photo induced reduction [79], thermal reduction and hydrogen reduction. We aimed to achieve this by the use of ALD.

ALD has recently gained popularity because of its precise deposition at the atomic level.[80] Unlike other physical and chemical deposition methods, ALD depends on self-limiting chemical reactions; only one layer can be adsorbed on the substrate for reaction per cycle. The titanium precursor used for ALD is expected to bind to oxygen functional groups such as hydroxyl (-OH) and carboxylic (-COOH) groups. Graphene oxide is rich in these oxygen functional groups, making it an ideal substrate for ALD of TiO_2. By controlling the temperature of ALD chamber and precursor pulsing time, we were able to control the resulting TiO_2 phase and deposition rate. The number of ALD cycle is varied to render different thicknesses.

This study investigates the catalytic activities of titanium dioxide (TiO_2) incorporated GO, which was achieved by ALD. The catalytic activity was systematically evaluated by CV curves. It was found that TiO_2-anchored GO (by ALD) exhibits a catalytic

activity significantly higher than rGO itself. The temperature for ALD process also was found to effect the catalytic activity of resulting TiO_2/rGO. This is ascribed to a combined contribution from facilitated reduction of GO and higher deposition rate of TiO_2 during ALD. In addition, there is an optimal amount of TiO_x for catalytic activity, which is achieved by 25 cycles of ALD. The deposition of TiO_x onto GO by ALD is not new, but to our knowledge this is the first study to take this approach for ORR catalysis.

4.2 Methods

GO is synthesized using graphite by a modified version of Hummer's method.[81] The GO solution is then brought to a pH > 5 by several water rinses followed by centrifuge, and vacuum filtrated to a solid. The GO is then dispersed in 1:9 water to dimethylformamide (DMF) to make a 2 M solution.

GO solution is then drop-casted on the surface of stainless steel (SS). The SS is prepared and cleaned using a three-step solvent rinse with isopropanol, ethanol and water. The SS submerged in each solvent is sonicated for 20 min and finalized with ozone cleaning. The drop casting process consisted of covering the surface SS with 10 ml of the GO colloidal solution followed by an air-drying at room temperature. This dropcasting-and-drying process was repeated eight times to prepare a GO/SS scaffold for TiO_2 ALD onto it.

Before inserting the GO/SS sample into the ALD chamber (Savanah 100, Cambridge NanoTech), the chamber is heated up to the desired temperature. The deposition was performed at three different temperatures (150, 200 and 250°C) with

different number of ALD cycles (10 – 125). The pulsing time for titanium precursor, Tetrakis (dimethylamido) titanium, was maintained at 0.5 s and the water (as oxygen source) was maintained at 0.1 s. The deposition was performed under a vacuum conditions with N_2 flow. It is estimated that 25 cycles lead to a TiO_x deposition with a nominal thickness of ~1 nm.

CV measurements were performed with the catalyst (TiO_2 ALD'ed GO) in 0.1 M KOH electrolyte. Ag/AgCl was used as the reference electrode, and Pt wire was used as the counter electrode. The scan rate was 20 mV/sec, with a potential window of -0.3 to 0.7 V, under oxygen and nitrogen purged environments using a Biologic Potentiostat. All samples were tested after dropcasting a catalyst ink on a glassy carbon electrode. The ink were a mixture of the TiO_2/rGO catalyst and 5 wt% Nafion in a solvent made of 1:1 water and DMF.

4.3 Results and Discussion

The SEM image in Figure 7 obtained at a low voltage using an in-lens detector reveals the morphology of GO sheets obtained from the modified Hummer's method. The GO structure is folded sheets that are wrinkled throughout the SS substrate.

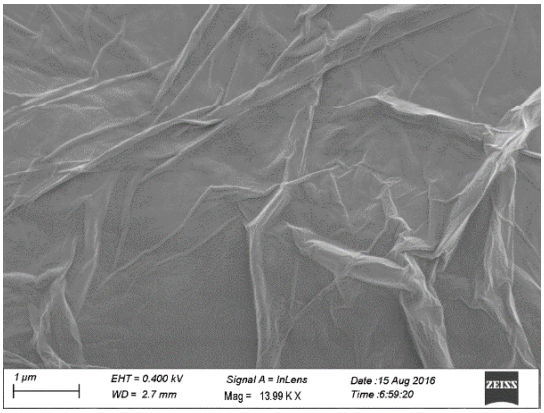

Figure 7. An SEM image of GO on the SS revealing a sheet-like morphology of GO.

The FTIR spectrum shown in Figure 8 indicates the abundance of oxygen-containing functional groups on GO. These oxygen functional groups are conjectured to be responsible for binding the Ti precursor during ALD. The FTIR result shows distinct carbonyl peak, which can be responsible for carboxylic functional group at around 1625 cm^{-1}, and a distinct hydroxyl (-OH) peak at around 3400 cm^{-1}.

The synthesis of GO by a modified form of Hummer's method was proven to be successful based on the SEM (Figure 7) and FTIR results (Figure 8). The goal of using Hummer's method is to synthesize carbon structures rich in oxygen functional group that TiO_x can bind to during the ALD,[81] which was successfully achieved. GO, due to high density of defects, is not a conductive material, but it was chosen for its simple processing, stable mechanical properties and the flexibility. More importantly, it has the flexibility of being readily functionalized and reduced. Even though GO itself has low conductivity, which is not ideal for catalytic material, the functionalization and reduction of GO can enhance its conductivity.[82,16]

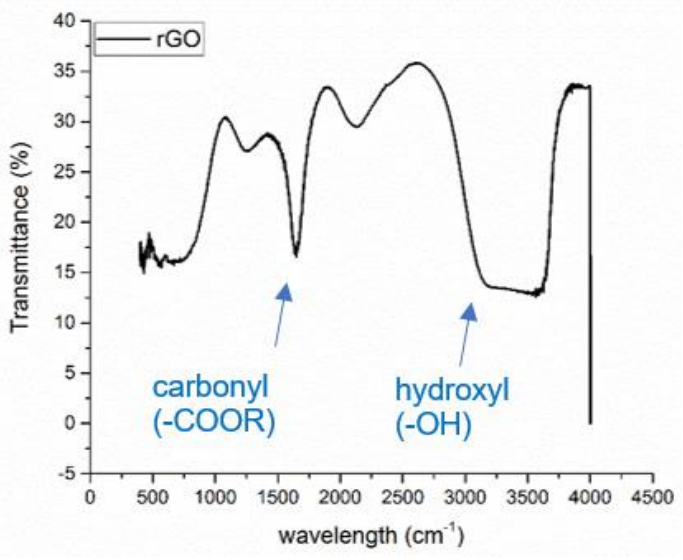

Figure 8. An FTIR spectrum showing oxygen functional groups on GO.

After TiO_2 was deposited by ALD onto the GO/SS, energy dispersive spectroscopy (EDS) was performed to examine the presence of titanium. The EDS spectra in Figure 9 shows two small peaks corresponding to titanium, confirming that Ti is indeed deposited by ALD on the surface of the GO. A distinct Fe peak in the spectra is ascribed to the SS substrate.

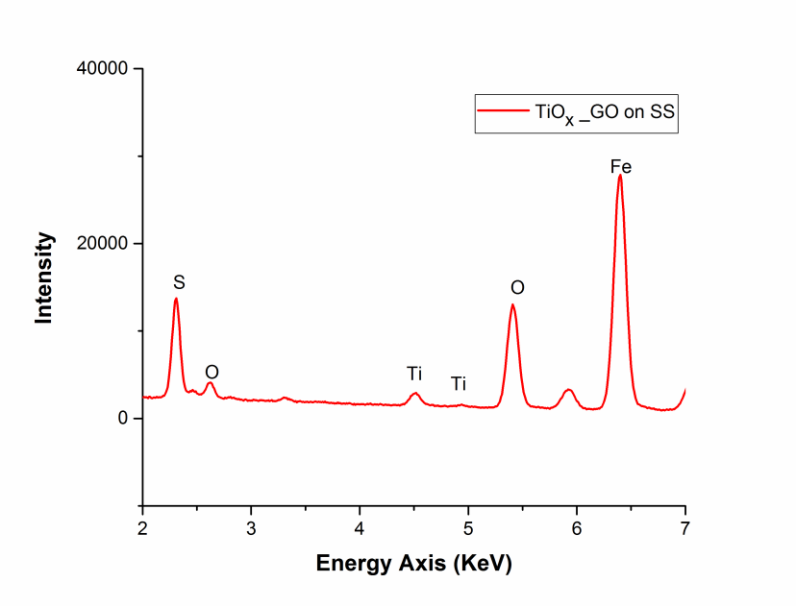

Figure 9. EDS map of the elemental composition found in the TiO_2/GO material

Transmission electron microscopy (TEM) was used to image the morphology of the GO and TiO_2 nanoparticles formed by the ALD. The sheet-like graphene structure was still conserved even after ALD was performed at elevated temperatures. However, embedded in the GO sheet-like structure there are nanoparticles that are several nanometers wide (**Figure 10** a-c). With the use of energy filtered transmission electron microscopy (EFTEM), the nanoscale particles correspond to TiO_2 (**Figure 10** d).

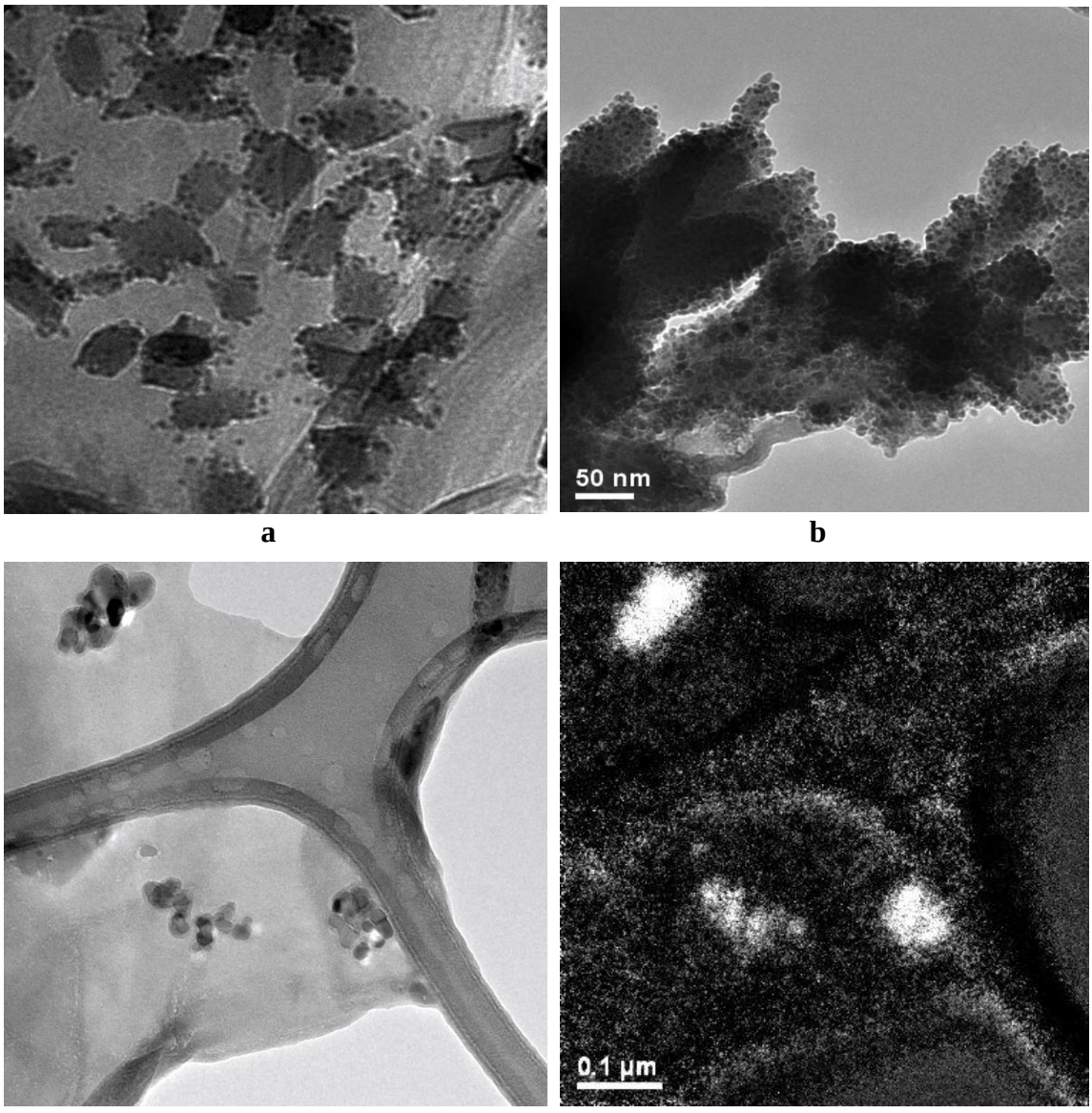

Figure 10. (a-c) TEM images of the TiO_2 incorporated GO by ALD. (d) An energy filtered TEM image that reveals the nanoparticles correspond to TiO_2.

When exposed to high temperatures during ALD, GO is likely to turn into reduced graphene oxide (rGO), which is more conductive.[83] In addition, TiO_2 binds to oxygen functional groups on GO, which is considered to be another contribution toward GO

reduction. On the other hand, by binding TiO_2 nanoparticles, GO nanosheets can be free of the issue of being agglomerated.[84] As an agglomeration can cause a decrease in the overall surface area and thus a sacrifice in the overall catalytic activity per gram, the suppression of agglomeration is highly advantageous for catalytic performance.

CV results in Figure 11 exhibits a comparison of electrochemical activity between TiO_2/rGO and GO. There is a significant different in the ORR performance between the two samples in terms of current density (0.1 mA/cm^2 for GO; ~ 0.5 mA/cm^2 for TiO_2/rGO) and on-set potential (-0.18 V vs Ag/AgCl for GO; -0.02 V for TiO_2/rGO), indicating that the ORR activity of GO was dramatically improved by TiO_2 ALD.

In addition,

Figure 12 shows the effect that different number of ALD cycles has on the ORR activity. The CV was taken of GO samples deposited with 12 cycles, 25 cycles and 125 cycles. All samples were deposited at 250°C. Looking at the on-set potential and current, we see that out of the three samples the sample deposited with 25 cycles has the best performance. The TiO_2/rGO deposited at 25 cycles has a current density of ~ 1 mA/cm^2, and an on-set potential of ~ -0.056 V vs Ag/AgCl. The tetrakis (dimethylamido) titanium precursor at 250°C is expected to have a deposition rate of 0.04 nm/cycle. Therefore, an estimated thickness of ~ 1 nm coating was enough to form the nanometer-sized TiO_2 nanoparticles seen in the TEM images, which exhibited the best catalytic performance. The 125 cycles, corresponding to the TiO_2 thickness of 5 nm, would result in the formation of film, as opposed to dispersed nanoparticles. Film in comparison to nanoparticles have smaller surface area, which can reduce the number of exposed active sites. When compared

to the benchmark Pt/C catalyst, the on-set potential was measured at ~ 0.015 V vs Ag/AgCl, slightly higher than that of the TiO_2/rGO catalyst.

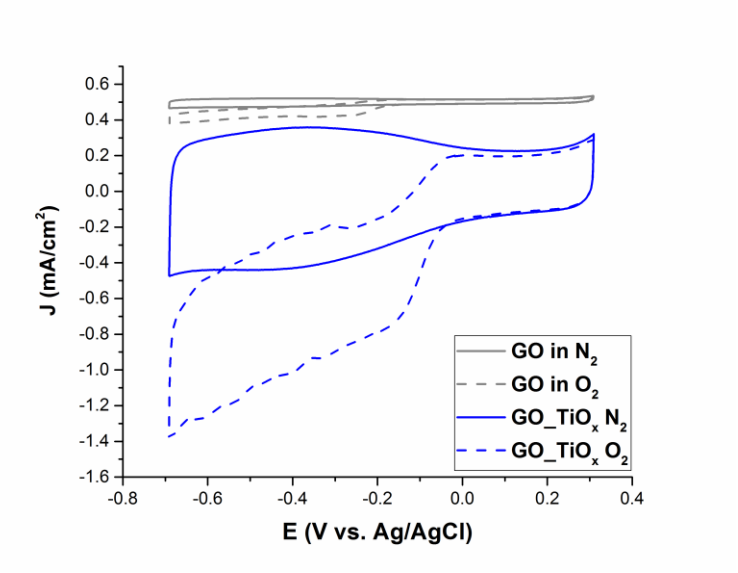

Figure 11. CV curves of GO and ALD TiO_2/GO in O_2 and N_2 saturated 0.1M KOH electrolyte.

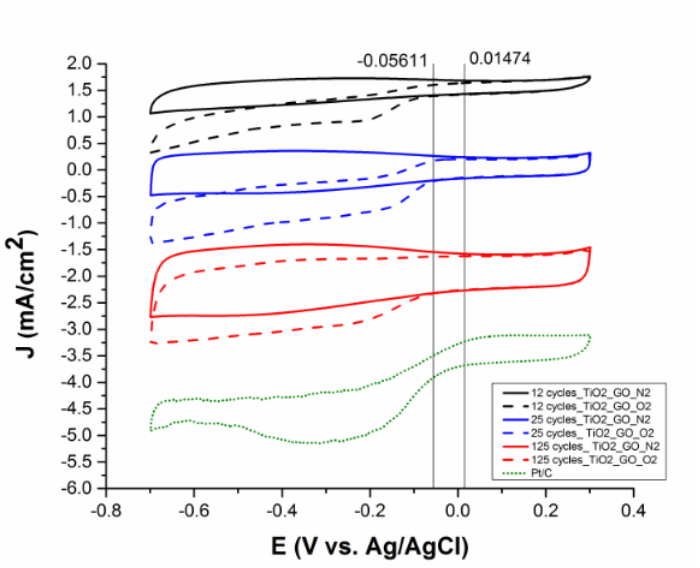

Figure 12. CV curves of TiO_2/GO deposited for different number of ALD cycles.

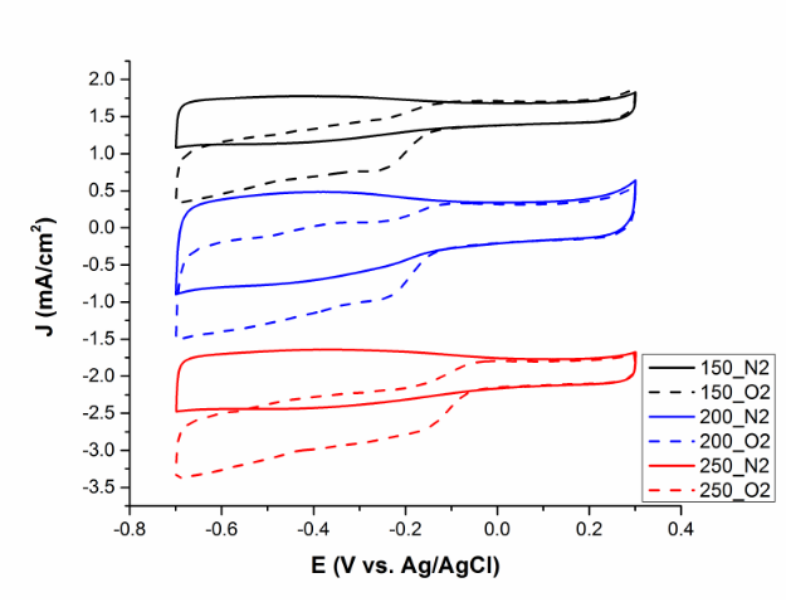

Figure 13. CV curves of TiO_2/GO deposited at different chamber temperatures (150, 200 and 250°C) by ALD.

The TiO_2/rGO samples were also deposited at three different chamber temperatures. The set of samples in

Figure 13 were all deposited with a cycle number of 25. From the CV measurements, it is evident that the overall performance of TiO_2/rGO was improved by increasing the chamber temperature during ALD. Deposition at a higher temperature not only increases the reduction of GO, but it also has an important role in form nucleation and crystal structure formation. Recall that catalytic activity of certain nanostructures has depended on what the oxidation state of the metal, crystal structure and crystal phase. This has especially been true for TiO_2, and the formation of non-stoichiometric form of TiO_2 has been shown to be better for its ORR catalytic activity by facilitating the absorption of O_2.[22]

4.4 Conclusion

This Chapter presents a study using CV for characterizing the catalytic activity of TiO_2/rGO. From TEM images, it was evident that TiO_2 nanoparticles (< 10 nm) were deposited by ALD. The CV results indicated a significant increase in catalytic activity after deposition of TiO_2 by ALD. The optimal ALD condition for ORR catalysis was found to be 25 cycles of deposition at 250 °C. An excessive number of cycles is conjectured to result in a relatively low-surface-area structure while a small cycle number cannot disperse sufficient TiO_2 nanoparticles for an optimum catalysis. Even with the same cycle number, the reaction temperature is also found to have a significant impact on the ORR activity of resulting TiO_2/GO hybrid. A higher temperature is advantageous in further reducing GO (and thus improving electronic conductivity of resulting rGO) and facilitating nucleating and crystalline growth of TiO_2 particles. Any impact on the stoichiometry of TiO_2 particles itself can be a possible factor, which is yet to be revealed.

CHAPTER 5. CO-CU BIMETALLICA METAL ORGANIC FRAMEWORK FOR ELECTROCATALYSIS

5.1 Introduction

Metal organic frameworks (MOFs) have garnered wide attention for their ability to efficiently catalyze reactions such as water oxidation (which includes OER and HER) and ORR.[42,85,24] There are many properties associated with MOFs that are beneficial for catalysis purpose including: 1. highly porous structure for enhanced diffusion, 2. high surface area 3. improved adsorption of reactants, 4. chemical stability, 5. thermal stability and 6. high conductivity.[86] In addition, the facile synthesis, robust nature and use of abundant materials that are inexpensive, such as transitional metals and organic ligands, help make MOFs a promising material to use for electrocatalysis of water oxidation and oxygen.

MOFs are crystalline structures that are formed by coordination bonds between metal ions and organic ligands. When complexed with organic ligands to form the MOFs, the metal ions are atomically distributed into organized arrays, which can result in uniformly distributed active sites. Depending on the ligand and metal complex, there can be different lengths between the metal centers, which allow for tuning well defined void spaces that allow MOFs to have better diffusion, adsorption, selectivity and larger surface areas.[87] Changing the MOFs' pore size and composition alter its selectivity towards certain reaction,[88] and expected to affect the overall electrocatalytic performance of the MOF.[89]

Depending on the coordination of the metal, its electron configuration can be arranged to have favorability towards binding oxygen molecules or water molecules. [90] Using DFT calculations, researchers studied the rate limiting steps of each process of catalysis including adsorption, dissociation and desorption, and construct Gibbs free energy diagrams that serve as supplementary evidence to explain why certain metal ion-ligand arrangements provide more energetically favorable electrochemical process at each step these reactions.[56]

Metals such as Fe, Co, Ni, Cu and other transition metals have shown to have distinctive performance as electrocatalyst when used as metal clusters for MOFs.[62,91,92] Most recently, there was a report showing that an MOF with multiple metals can further enhance the electrocatalytic properties of an MOF because of the different filled energy states that add a dynamic that improves certain process during OER.[93]

Though often because of their pristine structure and high porosity, MOFs have deterred conductivity.[86] The issue with conductivity can be mitigated by incorporating the MOFs with conductive material like graphene, carbon nanotubes or other conductive material. For some MOFs and other coordinated structures, their incorporation into these supporting structures not only improves their electrocatalytic activity but also enables these structures to have bifunctional properties.[94,21] The improved catalytic performance of the composite is a result of the electron accepting ability of the supporting structures and the high surface area, which facilitate the overall electron transfer rate during catalysis.[24] The synergistic effect of metallic complex and the supporting material, which often leads to an improvement in framework stability, and encapsulation by the supporting material can provide the chemical stability necessary for operating in an acidic environment.[52,24] In

addition to serving as good electron conducting materials, structures such as graphene can coordinate with the ligands and act as struts that link MOF nodes.[95]

Another method for enhancing the catalytic performance of MOFs is to dope the MOFs with elements like nitrogen, phosphorus and sulfur. The ligands themselves can also provide dopants that can increase the number of charge carriers and increase the overall conductivity of the MOF material of interest.[96,97]

There are also ways of enhancing of MOFs properties without adding other materials by creating defects or vacancies in the MOF that will expose catalytic sites or increase the mobility of charge carriers within the MOF material. One way of creating defects in a MOF structure is pyrolysis or carbonization.[98] After pyrolysis, some materials have either rearranged their crystal structure to either expose catalytic sites by unsaturation of ligand to metal ion bonding, or by rearranging the structure to benefit catalytic activity.[99] Even though MOFs are generally thermally stable at relatively high temperatures, it is still possible to remove the metal ions in the MOF by acid treatment. The resulting metal-free structures have shown an electrocatalytic activity toward water oxidation and ORR even greater than those with the metal ions of high catalytic activity.[100] Some metal-free MOFs are not thermally stable, and therefore their distinct ordered arrays and complexes might be lost at high temperatures.[101]

It is also possible to create catalytically active sites by leaving metal atoms coordinatively unsaturated with ligands.[93] Both experimental results and DFT calculations revealed the existence of unsaturated metal sites, which are believed to play as open sites for adsorption and subsequent catalytic process. This leads to different metal ligand coordination that are more energetically favorable to reactant adsorption and reactant

dissociation towards the final product.[102] Similarly, methods such as oxygen plasma or other etching techniques can lead to unsaturated bonding and enhanced catalytic activity.[103]

In this study, cobalt-copper bimetallic MOF on graphene oxide (Co-Cu-NBDC-GO) was synthesized by a solvothermal method. This bimetallic structure can lead to mixed valence states where one metal can promote the adsorption and dissociation of specific reactant while the other metal induces an electron transfer that will enhance the interaction of the first metal with the desired reactants.[12,82] In addition, the amine groups found in the organic linker have the potential of embedding into the structure after heat treatment.[40,37] Not only does the bimetallic cobalt-copper MOF provide the needed chemical and physical structure, but also serves a template that will further enhance the catalytic performance by heat treatments at 600ºC and 700ºC in a controlled environment. The resulting bimetallic copper-cobalt GO complex (denoted as Co-Cu-NBDC-GO-600 and Co-Cu-NBDC-GO-700, respectively) exhibits decent catalytic capabilities towards both ORR and OER. Physical and electrochemical properties of the samples were characterized by SEM, CV and LSV with RDE and interpreted.

5.2 Methods

GO is synthesized using graphite powder by a modified Hummer's method.[81] The GO solution is then brought to a pH > 5 by several water rinses followed by centrifugation. It was then dispersed in ethanol to make 2 M colloidal solution, which was freeze-dried at -40ºC resulting in a porous brown solid GO.

0.75 mmol of $CoCl_2 \cdot 6H_2O$ (98%, purchased from Alfa Aesar) and 0.75 mmol $CuCl_2 \cdot 2H_2O$ (99+% ACS grade, purchased from Alfa Aesar) were dissolved in 10 ml of

dimethylformamide (DMF, 99.8+% ACS grade, purchased from Alfa Aesar) and sonicated for 20 min. Then 1.5 mmol of 2-aminoterephthalic acid (NBDC) (99%, ACS grade, purchased from Alfa Aesar) was added to the Co-Cu solution and sonicated for additional 20 min. 5wt% of freeze-dried GO was then added to the mixture and sonicated for 20 min. The solution was transferred to a 40 ml autoclave for the solvothermal reaction at 140ºC for 48 hrs under airtight conditions. The solid was collected and rinsed several times via centrifugation and dried at 150ºC under N_2 conditions. Co-Cu-NBDC-GO-600 and Co-Cu-NBDC-GO-700 were synthesized by annealing Co-Cu-NBDC-GO at 600 and 700ºC for 2 hr in N_2 environment. Co-Cu-GO was prepared in the same way as Co-Cu-NBDC-GO, but without NBDC.

SEM was used to image the morphology of the samples before and after annealing. Images were taken at an acceleration voltage ranging 0.5 kV to 1.25 kV. The ORR performance of the samples was evaluated using CV in a three-electrode set-up with a Ag/AgCl reference electrode and a potential rate of 20 mV/s. The samples are tested are under N_2 saturation to obtain a background scan, and then under saturated O_2 to see the ORR. LSV measurements were performed on an RDE setup. The ORR LSV curves were measured using 20 mV/sec and at 1600 rpm, and the OER LSV was performed at 5 mV/sec at 1600 rpm, both under oxygen environment. All samples were made into a catalyst ink by dissolving the solid electrocatalyst sample in ethanol and adding 1:1 weight ratio of Nafion. All measurements had a loading mass of ~0.4 mg/cm^2.

5.3 Results and Discussion

The Co-Cu-NBDC structure shows a flower-like morphology with petal-like flakes of ~ 50 nm thickness (Figure 5.1c). Even after annealing, a similar overall morphology was observed (Figure 5.1b). The hierarchical morphology is desirable for efficient catalysis because the macro-pores allow fluent mass transport and the petal-like structure achieves a higher surface area.

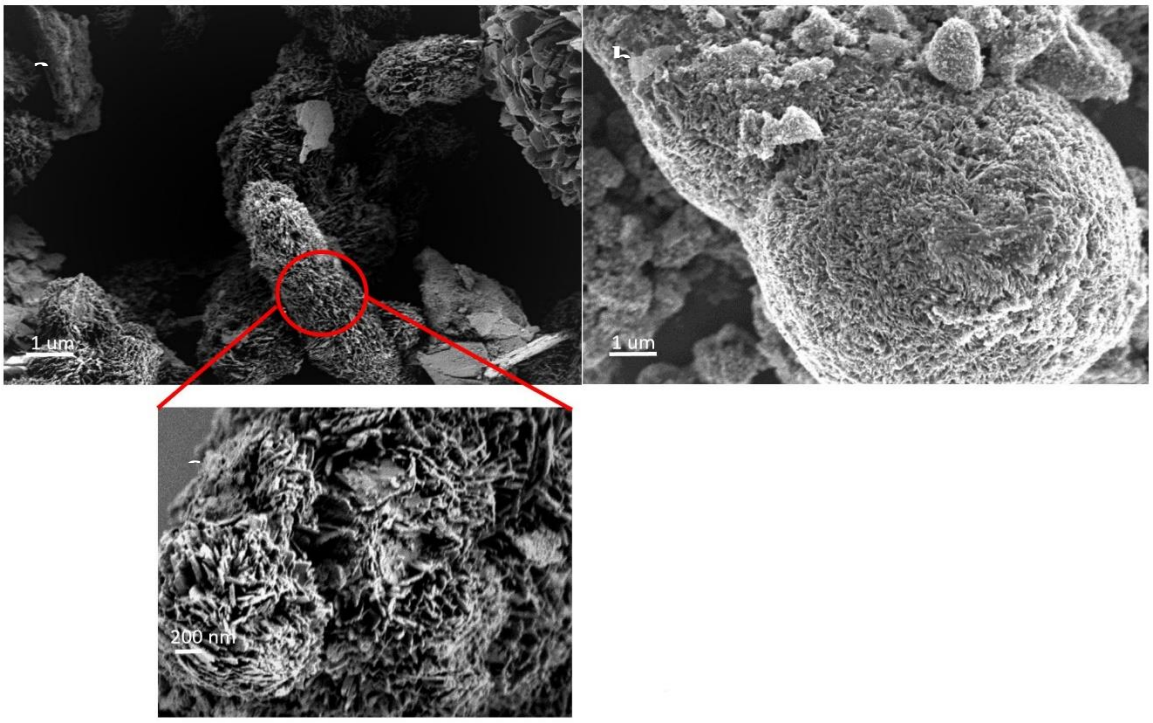

Figure 14. shows SEM images of a) and c) Co-Cu-NBDC, b) Co-Cu-NBDC-600ºC

To study the role of each component in the bimetallic MOF structures, CV was performed on Co-Cu-NBDC, Co-NBDC-GO and Co-Cu-NBDC-GO samples, all annealed at 600°C, and Pt/C as a control sample (Figure 5.2). The role of GO is significant as evident from the CV curves. The addition of GO resulted in a larger capacitance, and thus a larger surface area (Figure 14a). In addition, the on-set potential and the current density are

enhanced significantly by merging with GO. Essentially, the on-set potential defines the minimum amount of overpotential to incur ORR. The further away the on-set potential is from the reversible potential of oxygen electrocatalysis (1.23 V vs RHE), the more voltage loss is incurred to have the reaction occur. The on-set potentials of Co-Cu-NBDC and Co-Cu-NBDC-GO were quantified to be ~0.65 V and ~0.81 V, respectively. From these observations, it is shown that the GO not only acts as a support but enhance the surface area and catalytic activity toward ORR.

The excellent ORR performance for Co-Cu-NBDC-GO is also a result of the bimetallic nature of this MOF material. The role of Cu is evident when comparing Co-Cu-NBDC-GO with Co-NBDC-GO. While the two samples show similar on-set potentials, Co-Cu-NBDC-GO exhibits significantly larger surface area and current density than those of Co-Cu-NBDC (Figure 15). This in part is due to the larger surface area of Co-Cu-NBDC-GO; Co-NBDC-GO do not have the flower-like structure.

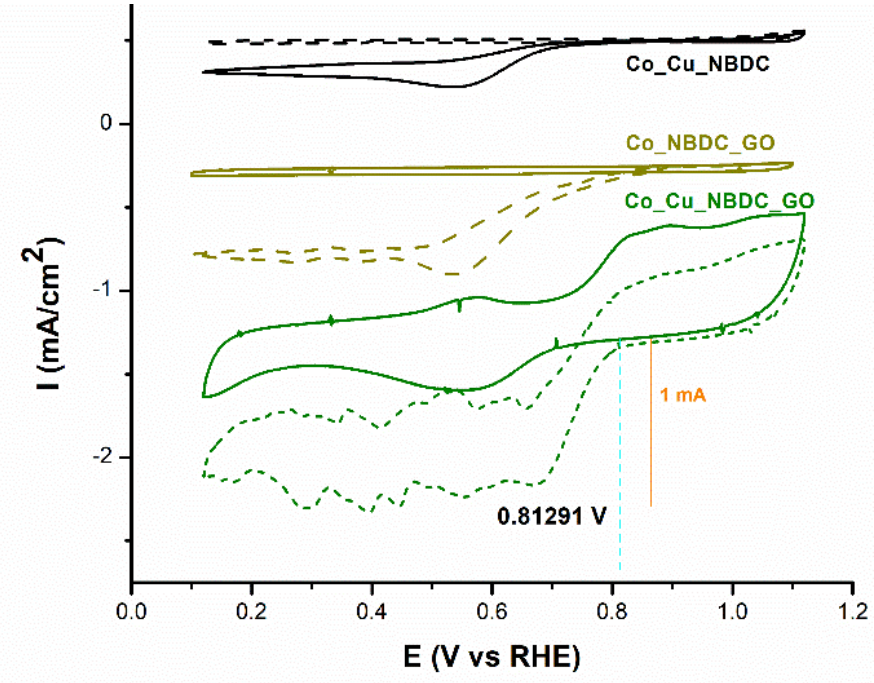

Figure 15 CV curves of Co-Cu-NBDC, Co-NBDC-GO and Co-Cu-NBDC-GO samples; Pt/C was studied as a reference sample.

The post-annealing temperatures also influenced the overall performance for Co-Cu-NBDC-GO. An increase of annealing temperature increased capacitance surface area, current density and on-set potential (Figure 16). Co-Cu-NBDC-GO annealed at 700°C (Co-Cu-NBDC-GO-700) had an on-set potential of 0.822 vs RHE.

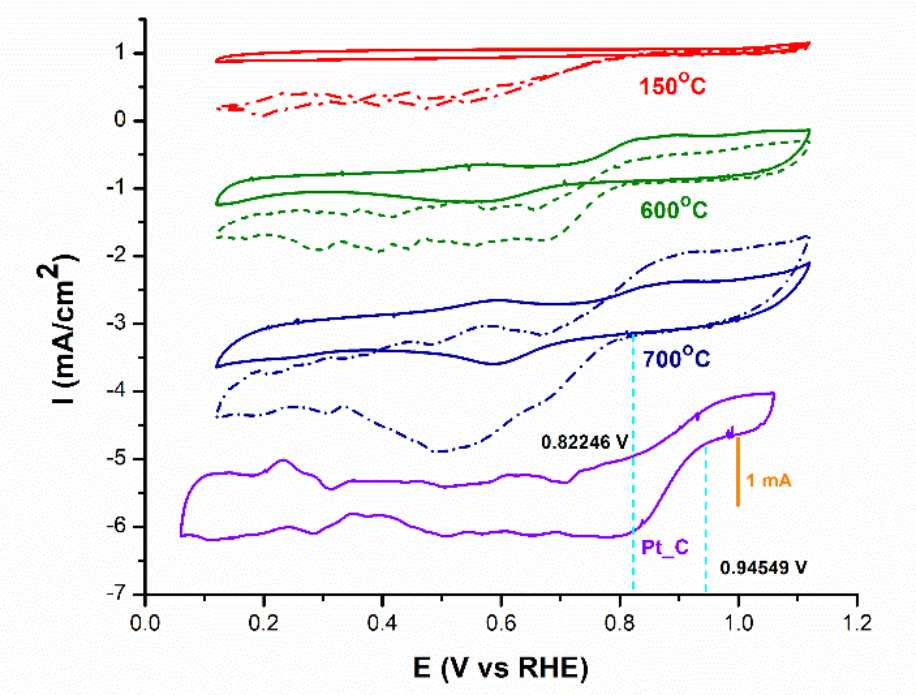

Figure 16 CV curves of Co-Cu-NBDC-GO dried at 150°C and annealed at 600°C and 700°C. CV curve of Pt/C is presented for comparison purpose.

The half-way potential of Co-Cu-NBDC-GO-700 was around 0.72 V vs RHE and for Pt-C it was 0.82 V vs RHE (Figure 17a). The Tafel slope was determined by fitting a line to the kinetic region at higher over potential values. The slope for Co-Cu-NBDC-700 was -78.87 mV/dec, which for Pt-C it was -52.42 mV/dec (Figure 17b).

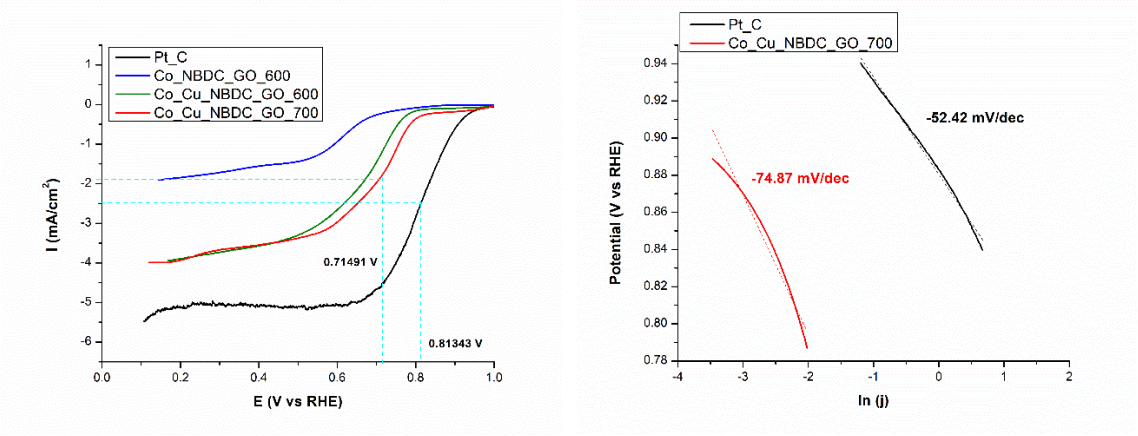

a **b**

Figure 17. a) shows the ORR LSV using RDE at 1600 rpm under oxygen saturation in 0.1 M KOH b) shows the Tafel slope of Co-Cu-NBDC-GO and Pt-C to measure oxygen evolution reactions (OER).

The OER catalytic capabilities were also measured using LSV (Figure 18a). The on-set potential at 10 mA/cm^2 for Co-Cu-NBDC-GO-700 was 1.57 V vs RHE. For the other samples, including Pt/C, their on-set potential was higher indicating a higher overpotential for OER. The LSV curve was used to find the Tafel slope; for Co-Cu-NBDC-GO-600 and Co-Cu-NBDC-GO-700, it is 56.57 and 46.44 mV/dec, respectively (Figure 18b). The difference between the on-set potentials of ORR and OER was around 0.86 V, which is comparable to other reported high-performance bifunctional electrocatalysts.[21]

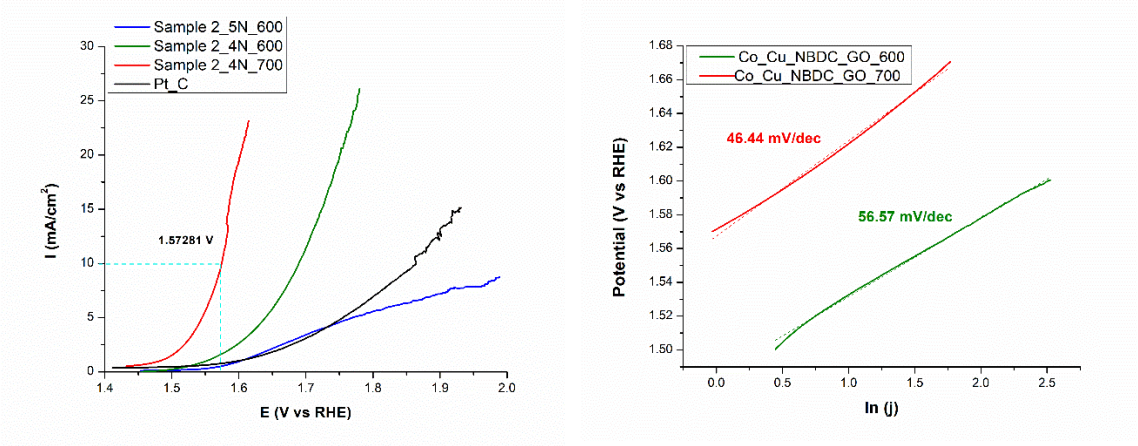

a **b**

Figure 18 a) OER LSV using RDE at 1600 rpm in oxygen saturated 0.1 M KOH b) Tafel slope of Co-Cu-NBDC-GO-600 and Co-Cu-NBDC-GO-700 for OER.

5.4 Conclusion

In this study, cobalt-copper bimetallic MOF was synthesized by a solvothermal method with and without the introduction of GO, their catalytic performance for OER and ORR was analyzed. The overall catalytic activity of the MOF was found positively affected by the bimetallic nature of the MOF. The performance is further enhanced by an introduction of GO, which not only increased the surface area for reaction but also improved on-set potential and current density. The beneficial effect of bimetallic coordination was reflected in terms of capacitance area and current gain. Mixed valence states caused by the bimetallic coordination is conjectured to have facilitated dissociation of reactants and charge transfer process. The post-annealing procedure was also found to have a significant impact on the performance for both ORR and OER. In general, a higher annealing temperature resulted in a performance for both ORR and OER, in terms of on-set potential and Tafel slope. The potential difference between $E_{ORR,1/2}$ and $E_{OER,j=10}$

obtained from Co-NBDC-GO-700 was ~0.86 V, which proves its promise as a bifunctional oxygen electrocatalyst.

CHAPTER 6. CONCLUSION

In this thesis, two different methods were applied to synthesize inorganic/organic hybrid catalysts for ORR and OER: ALD-based metal oxide anchoring and a solvothermal approach. The electrocatalytic performance of the resulting hybrid catalysts was characterized, and relevant discussions were provided.

The first study investigated the catalytic activities of TiO_2 incorporated GO by ALD. The catalytic activity was systematically measured by CV. TiO_2 nanoparticles sized < 10 nm were successfully deposited evenly on GO surface by ALD. A higher number of ALD cycles resulted in an overall better ORR performance in terms of on-set potential and active surface area. At 25 ALD cycles, the performance, especially in terms of on-set potential, reaches an optimum. It was also found that the chamber temperature for ALD process renders a positive impact on the catalytic performance when the same ALD cycle number of 25 was used. It is conjectured that a higher temperature resulted in a further reduction of GO (and thus an improved electronic conductivity of graphene scaffold) and a facilitated nucleation and crystallization of TiO_2 nanoparticles.

In the second study, a bimetallic MOF was synthesized using cobalt and copper chloride, complexed with 2-aminoterephthalic acid with and without mixing with GO. The catalytic performance for ORR and OER was characterized, and related analysis was performed. First, the overall catalytic performance was found much enhanced by the introduction of GO in terms of on-set potential and current density. The beneficial effect of bimetallic coordination was also reflected in terms of capacitance area and current gain. Mixed valence states caused by the bimetallic coordination is conjectured to have

facilitated dissociation of reactants and charge transfer process. A post-annealing procedure with a higher annealing temperature rendered a better performance for both ORR and OER, in terms of on-set potential and Tafel slope. The potential difference between $E_{ORR,1/2}$ and $E_{OER,j=10}$ obtained from Co-NBDC-GO-700 was ~0.86 V, which proves its promise as a bifunctional oxygen electrocatalyst.

While the aforementioned studies show promises of each organic/inorganic hybrid material as an oxygen electrocatalyst, an in-depth mechanism study to reveal the process-property-performance correlation is expected to provide a useful insight in designing high-performance catalysts from these approaches.

REFERENCES

1. K. Aleklett, M. Lardelli, O. Qvennerstedt, Peeking at peak oil, Springer, (2012)

2. Paul, B. & Andrews, J. PEM unitised reversible/regenerative hydrogen fuel cell systems: State of the art and technical challenges. *Renew. Sustain. Energy Rev.* **79,** 585–599 (2017).

3. Winter, M. & Brodd, R. J. What are batteries, fuel cells, and supercapacitors? *Chem. Rev.* **104,** 4245–4269 (2004).

4. Lopes, T., Kucernak, A., Malko, D. & Ticianelli, E. A. Mechanistic Insights into the Oxygen Reduction Reaction on Metal – N – C Electrocatalysts under Fuel Cell Conditions. 1580–1590 (2016). doi:10.1002/celc.201600354

5. Han, L., Dong, S. & Wang, E. Transition-Metal (Co, Ni, and Fe)-Based Electrocatalysts for the Water Oxidation Reaction. *Adv. Mater.* **28,** 9266–9291 (2016).

6. Serov, A., Artyushkova, K. & Atanassov, P. Fe-N-C oxygen reduction fuel cell catalyst derived from carbendazim: Synthesis, structure, and reactivity. *Adv. Energy Mater.* **4,** 1–7 (2014).

7. Dai, L., Xue, Y., Qu, L., Choi, H.-J. & Baek, J.-B. Metal-Free Catalysts for Oxygen Reduction Reaction. *Chem. Rev.* **115,** 4823–4892 (2015).

8. Masa, J., Xia, W., Muhler, M. & Schuhmann, W. On the Role of Metals in Nitrogen-

Doped Carbon Electrocatalysts for Oxygen Reduction. *Angew. Chemie Int. Ed.* **54,** 10102–10120 (2015).

9. Shui, J., Wang, M., Du, F. & Dai, L. N-doped carbon nanomaterials are durable catalysts for oxygen reduction reaction in acidic fuel cells. *Sci. Adv.* 1–7 (2015).

10. Barbir, F., Molter, T. & Dalton, L. Efficiency and weight trade-off analysis of regenerative fuel cells as energy storage for aerospace applications. *Int. J. Hydrogen Energy* **30,** 351–357 (2005).

11. Chen, G., Bare, S. R. & Mallouk, T. E. Development of Supported Bifunctional Electrocatalysts for Unitized Regenerative Fuel Cells. *J. Electrochem. Soc.* **149,** A1092 (2002).

12. Alayoglu, S., Nilekar, A. U., Mavrikakis, M. & Eichhorn, B. Ru–Pt core–shell nanoparticles for preferential oxidation of carbon monoxide in hydrogen. (2008). doi:10.1038/nmat2156

13. Gorlin, Y. & Jaramillo, T. F. A Bifunctional Nonprecious Metal Catalyst for Oxygen Reduction and Water Oxidation. doi:10.1021/ja104587v

14. Liang, Y. *et al.* Co 3 O 4 nanocrystals on graphene as a synergistic catalyst for oxygen reduction reaction. (2011). doi:10.1038/NMAT3087

15. Ding, J., Zhou, Y., Li, Y., Guo, S. & Huang, X. MoS 2 Nanosheet Assembling Superstructure with a Three- Dimensional Ion Accessible Site: A New Class of Bifunctional Materials for Batteries and Electrocatalysis.

doi:10.1021/acs.chemmater.5b04815

16. Qu, L., Liu, Y., Baek, J.-B. B. & Dai, L. Nitrogen-doped graphene as efficient metal-free electrocatalyst for oxygen reduction in fuel cells. *ACS Nano* **4,** 1321–1326 (2010).

17. Grigoriev, S. A. *et al.* Design and characterization of bi-functional electrocatalytic layers for application in PEM unitized regenerative fuel cells. *Int. J. Hydrogen Energy* **35,** 5070–5076 (2009).

18. Yang, H., Zhang, Y., Hu, F. & Wang, Q. Urchin-like CoP Nanocrystals as Hydrogen Evolution Reaction and Oxygen Reduction Reaction Dual-Electrocatalyst with Superior Stability. *Nano Lett.* **15,** 7616–7620 (2015).

19. Duan, J., Chen, S. & Zhao, C. Ultrathin metal-organic framework array for efficient electrocatalytic water splitting. *Nat. Commun.* (2017). doi:10.1038/ncomms15341

20. Cao, X. *et al.* Metal oxide-coated three-dimensional graphene prepared by the use of metal-organic frameworks as precursors. *Angew. Chemie - Int. Ed.* **53,** 1404–1409 (2014).

21. Aijaz, A. *et al.* Co@Co3O4 Encapsulated in Carbon Nanotube-Grafted Nitrogen-Doped Carbon Polyhedra as an Advanced Bifunctional Oxygen Electrode. *Angew. Chemie - Int. Ed.* **55,** 4087–4091 (2016).

22. Pei, D.-N. *et al.* ARTICLE Defective titanium dioxide single crystals exposed by high-energy {001} facets for efficient oxygen reduction. (2015).

doi:10.1038/ncomms9696

23. Close, T., Tulsyan, G., Diaz, C. a, Weinstein, S. J. & Richter, C. Reversible oxygen scavenging at room temperature using electrochemically reduced titanium oxide nanotubes. *Nat. Nanotechnol.* **10,** 418–22 (2015).

24. Jahan, M., Liu, Z. & Loh, K. P. A graphene oxide and copper-centered metal organic framework composite as a tri-functional catalyst for HER, OER, and ORR. *Adv. Funct. Mater.* **23,** 5363–5372 (2013).

25. Hod, I. *et al.* A porous proton-relaying metal-organic framework material that accelerates electrochemical hydrogen evolution. *Nat. Commun.* **6,** 1–9 (2015).

26. Wu, H.-W. A review of recent development: Transport and performance modeling of PEM fuel cells. (2016). doi:10.1016/j.apenergy.2015.12.075

27. Zhao, S., Yan, L., Luo, H., Mustain, W. & Xu, H. Recent progress and perspectives of bifunctional oxygen reduction/evolution catalyst development for regenerative anion exchange membrane fuel cells. *Nano Energy* **47,** 172–198 (2018).

28. Yan, D. *et al.* Defect Chemistry of Nonprecious-Metal Electrocatalysts for Oxygen Reactions. *Adv. Mater.* **29,** 1–20 (2017).

29. Morozan, A., Jousselme, B. & Palacin, S. Low-platinum and platinum-free catalysts for the oxygen reduction reaction at fuel cell cathodes. *Energy Environ. Sci.* **4,** 1238 (2011).

30. Doyle, R. L. & Lyons, M. E. G. *The Oxygen Evolution Reaction : Mechanistic*

Concepts and Catalyst Design. (2010). doi:10.1007/978-3-319-29641-8

31. Zhang, J., Zhao, Z., Xia, Z. & Dai, L. A metal-free bifunctional electrocatalyst for oxygen reduction and oxygen evolution reactions. *Nat. Nanotechnol.* **10,** 444–452 (2015).

32. Toda, T., Igarashi, H., Uchida, H. & Watanabe, M. Enhancement of the Electroreduction of Oxygen on Pt Alloys with Fe , Ni , and Co. **146,** 3750–3756 (1999).

33. Wei Seh, Z. *et al.* REVIEW SUMMARY Combining theory and experiment in electrocatalysis: Insights into materials design. doi:10.1126/science.aad4998

34. Kehlet, J. Trends in the exchange current for hydrogen evolution. 22–26 (2005). doi:10.1149/1.1856988

35. Li, M. *et al.* Ultrafine jagged platinum nanowires enable ultrahigh mass activity for the oxygen reduction reaction. *Science* **354,** 1414–1419 (2016).

36. Greeley, J. *et al.* Alloys of platinum and early transition metals as oxygen reduction electrocatalysts. *Nat. Chem.* **1,** 552–556 (2009).

37. Zou, X. *et al.* Cobalt-embedded nitrogen-rich carbon nanotubes efficiently catalyze hydrogen evolution reaction at all pH values. *Angew. Chemie - Int. Ed.* **53,** 4372–4376 (2014).

38. Mccrory, C. C. L., Jung, S., Peters, J. C. & Jaramillo, T. F. Benchmarking Heterogeneous Electrocatalysts for the Oxygen Evolution Reaction.

doi:10.1021/ja407115p

39. Fu, Y., Huang, Y., Xiang, Z., Liu, G. & Cao, D. Phosphorous-Nitrogen-Codoped Carbon Materials Derived from Metal-Organic Frameworks as Efficient Electrocatalysts for Oxygen Reduction Reactions. *Eur. J. Inorg. Chem.* **2016,** 2100–2105 (2016).

40. Hou, Y. *et al.* An advanced nitrogen-doped graphene/cobalt-embedded porous carbon polyhedron hybrid for efficient catalysis of oxygen reduction and water splitting. *Adv. Funct. Mater.* **25,** 872–882 (2015).

41. Gong, K., Du, F., Xia, Z., Durstock, M. & Dai, L. Nitrogen-doped carbon nanotube arrays with high electrocatalytic activity for oxygen reduction. *Science* **323,** 760–764 (2009).

42. Zhao, S. *et al.* Ultrathin metal-organic framework nanosheets for electrocatalytic oxygen evolution. *Nat. Energy* **1,** 1–10 (2016).

43. Xu, L. *et al.* Oxygen Vacancies Plasma-EngravedCo 3 O 4 Nanosheets with Oxygen Vacancies and High Surface Area for the Oxygen Evolution Reaction. doi:10.1002/ange.201600687

44. Amiinu, I. S. *et al.* Multifunctional Mo–N/C@MoS2 Electrocatalysts for HER, OER, ORR, and Zn–Air Batteries. *Adv. Funct. Mater.* **27,** 1–11 (2017).

45. Liang, Y., Wang, H., Casalongue, H. S., Chen, Z. & Dai, H. TiO 2 Nanocrystals Grown on Graphene as Advanced Photocatalytic Hybrid Materials. **3,** 701–705

(2010).

46. Wang, L. *et al.* Dendritic copper-cobalt nanostructures/reduced graphene oxide-chitosan modified glassy carbon electrode for glucose sensing. *Sensors Actuators, B Chem.* **195,** 1–7 (2014).

47. Yang, Z. *et al.* Sulfur-Doped Graphene as an Efficient Metal-free Cathode Catalyst for Oxygen Reduction. (2011). doi:10.1021/nn203393d

48. Zhang, J., Zhao, Z., Xia, Z. & Dai, L. A metal-free bifunctional electrocatalyst for oxygen reduction and oxygen evolution reactions. *Nat. Nanotechnol.* **10,** 444–452 (2015).

49. Yang, D.-S., Bhattacharjya, D., Song, M. Y. & Yu, J.-S. Highly efficient metal-free phosphorus-doped platelet ordered mesoporous carbon for electrocatalytic oxygen reduction. (2014). doi:10.1016/j.carbon.2013.10.065

50. Jia, Y. *et al.* Defect Graphene as a Trifunctional Catalyst for Electrochemical Reactions. *Adv. Mater.* **28,** 9532–9538 (2016).

51. Johansson, M. B. NiFeO X as a Bifunctional Electrocatalyst for Oxygen Reduction (OR) and Evolution (OE) Reaction in Alkaline Media. **3,** 1–26 (2018).

52. Jin, H. *et al.* In situ cobalt-cobalt oxide/N-doped carbon hybrids as superior bifunctional electrocatalysts for hydrogen and oxygen evolution. *J. Am. Chem. Soc.* **137,** 2688–2694 (2015).

53. Tao, L. *et al.* Creating coordinatively unsaturated metal sites in metal-organic-

frameworks as efficient electrocatalysts for the oxygen evolution reaction: Insights into the active centers. *Nano Energy* **41,** 417–425 (2017).

54. Wang, Y. *et al.* Reduced mesoporous Co3O4nanowires as efficient water oxidation electrocatalysts and supercapacitor electrodes. *Adv. Energy Mater.* **4,** 1–7 (2014).

55. Cheng, F. *et al.* Rapid room-temperature synthesis of nanocrystalline spinels as oxygen reduction and evolution electrocatalysts. (2011). doi:10.1038/NCHEM.931

56. Duan, J., Chen, S. & Zhao, C. Ultrathin metal-organic framework array for efficient electrocatalytic water splitting. *Nat. Commun.* **8,** 1–7 (2017).

57. Wang, Y., Tran, H. D., Liao, L., Duan, X. & Kaner, R. B. Nanoscale Morphology, Dimensional Control, and Electrical Properties of Oligoanilines. doi:10.1021/ja1014184

58. Peters, A. W., Li, Z., Farha, O. K. & Hupp, J. T. Atomically Precise Growth of Catalytically Active Cobalt Sulfide on Flat Surfaces and within a Metal-Organic Framework via Atomic Layer Deposition. *ACS Nano* **9,** 8484–8490 (2015).

59. O'Keeffe, M. & Yaghi, O. M. Deconstructing the crystal structures of metal-organic frameworks and related materials into their underlying nets. *Chem. Rev.* **112,** 675–702 (2012).

60. Chen, J., Lim, B., Lee, E. P. & Xia, Y. Shape-controlled synthesis of platinum nanocrystals for catalytic and electrocatalytic applications. *Nano Today* **4,** 81–95 (2009).

61. Nanostructures, Z. Zero-Dimensional Nanostructures: Nanoparticles 3.1. **c,** 51–81

62. Karthik, P., Pandikumar, A., Preeyanghaa, M., Kowsalya, M. & Neppolian, B. Amino-functionalized MIL-101(Fe) metal-organic framework as a viable fluorescent probe for nitroaromatic compounds. doi:10.1007/s00604-017-2215-2

63. Qu, Q. *et al.* Chemically Binding Carboxylic Acids onto TiO 2 Nanoparticles with Adjustable Coverage by Solvothermal Strategy. *Langmuir* **26,** 9539–9546 (2010).

64. Dai, X. *et al.* Molybdenum Polysulfide Anchored on Porous Zr-Metal Organic Framework to Enhance the Performance of Hydrogen Evolution Reaction. *J. Phys. Chem. C* **120,** 12539–12548 (2016).

65. Cundy, C. S. & Cox, P. A. The hydrothermal synthesis of zeolites: Precursors, intermediates and reaction mechanism. *Microporous Mesoporous Mater.* **82,** 1–78 (2005).

66. Pinna, N. & Knez, M. *Edited by Atomic Layer Deposition of Nanostructured Materials Related Titles Nanocomposites Bulk Nanostructured Materials Semiconductor Nanomaterials Handbook of Nitride Semiconductors and Devices Nanostructured Thin Films and Surfaces Electronic Material*. doi:10.1002/9783527639915

67. Neill, B. J. O. *et al.* Catalyst Design with Atomic Layer Deposition. *ACS Catal.* **5,** 1804–1825 (2015).

68. Lemaire, P. C., King, M. & Parsons, G. N. Understanding inherent substrate

selectivity during atomic layer deposition: Effect of surface preparation, hydroxyl density, and metal oxide composition on nucleation mechanisms during tungsten ALD. *J. Chem. Phys.* **146,** (2017).

69. Liu, Y., Deng, R., Wang, Z. & Liu, H. Carboxyl-functionalized graphene oxide–polyaniline composite as a promising supercapacitor material. *J. Mater. Chem.* **22,** 13619 (2012).

70. Lee, K. J., Elgrishi, N., Kandemir, B. & Dempsey, J. L. Electrochemical and spectroscopic methods for evaluating molecular electrocatalysts. *Nat. Rev. Chem.* **1,** (2017).

71. Asahi, R., Morikawa, T., Ohwaki, T., Aoki, K. & Taga, Y. Visible-Light Photocatalysis in Nitrogen-Doped Titanium Oxides. **293,** 269–272 (2001).

72. Wang, L. & Sasaki, T. Titanium oxide nanosheets: Graphene analogues with versatile functionalities. *Chem. Rev.* **114,** 9455–9486 (2014).

73. Ioroi, T., Siroma, Z., Fujiwara, N., Yamazaki, S. & Yasuda, K. Sub-stoichiometric titanium oxide-supported platinum electrocatalyst for polymer electrolyte fuel cells. **7,** 183–188 (2005).

74. Dreyer, D. R., Park, S., Bielawski, C. W. & Ruoff, R. S. The chemistry of graphene oxide. (2009). doi:10.1039/b917103g

75. Williams, G., Seger, B. & Kamat, P. V. TiO 2 -Graphene Nanocomposites. UV-Assisted Photocatalytic Reduction of Graphene Oxide. doi:10.1021/nn800251f

76. Pore, B. V. *et al.* Atomic Layer Deposition of Photocatalytic TiO 2 Thin Films From Titanium Tetramethoxide and Water **. 143–148 (2004). doi:10.1002/cvde.200306289

77. How, G. T. S., Pandikumar, A., Ming, H. N. & Ngee, L. H. Highly exposed {001} facets of titanium dioxide modified with reduced graphene oxide for dopamine sensing. *Sci. Rep.* **4,** 2–9 (2014).

78. Wang, X., Tabakman, S. M. & Dai, H. Atomic Layer Deposition of Metal Oxides on Pristine and Functionalized Graphene. *J. AM. CHEM. SOC* **130,** 8152–8153 (2008).

79. Williams, G., Seger, B. & Kamat, P. V. UV-Assisted Photocatalytic Reduction of Graphene Oxide. **2,** 1487–1491 (2008).

80. Reinke, M., Kuzminykh, Y. & Hoffmann, P. Surface Reaction Kinetics of Titanium Isopropoxide and Water in Atomic Layer Deposition. doi:10.1021/acs.jpcc.5b10529

81. Marcano, D. C. *et al.* Improved Synthesis of Graphene Oxide. **4,** (2010).

82. Liang, Y. *et al.* Covalent hybrid of spinel manganese-cobalt oxide and graphene as advanced oxygen reduction electrocatalysts. *J. Am. Chem. Soc.* **134,** 3517–3523 (2012).

83. Hayashi, T. *et al.* Temperature dependence of oxygen reduction mechanism on a titanium oxide-based catalyst made from oxy-titanium tetra-pyrazino-porphyrazine using carbon nano-tubes as support in acidic solution. *Electrochim. Acta* (2016).

doi:10.1016/j.electacta.2016.05.068

84. Ayissi, S. *et al.* Interaction of Titanium Oxide Nanostructures with Graphene and Functionalized Graphene Nanoribbons: A DFT Study. doi:10.1021/jp403835m

85. Zhu, C., Wang, K., Lei, T., Xiao, T. & Liu, L. Facile synthesis of MoS2/rGO-MOF hybrid material as highly efficient catalyst for hydrogen evolution. *Mater. Lett.* **216,** 243–247 (2018).

86. Furukawa, H., Cordova, K. E., O'Keeffe, M. & Yaghi, O. M. The chemistry and applications of metal-organic frameworks. *Science (80-.).* **341,** (2013).

87. Férey, G. Hybrid porous solids: past, present, future. doi:10.1039/b618320b

88. Sun, T., Ren, X., Hu, J. & Wang, S. Expanding Pore Size of Al-BDC Metal−Organic Frameworks as a Way to Achieve High Adsorption Selectivity for CO 2 /CH 4 Separation. doi:10.1021/jp411536d

89. Fan, W. *et al.* A Stable Amino-Functionalized Interpenetrated Metal−Organic Framework Exhibiting Gas Selectivity and Pore-Size-Dependent Catalytic Performance. doi:10.1021/acs.inorgchem.7b02148

90. Suntivich, J., May, K. J., Gasteiger, H. a, Goodenough, J. B. & Shao-horn, Y. A Perovskite Oxide Optimized for Molecular Orbital Principles. *Science (80-.).* **334,** 2010–2012 (2011).

91. Wang, R., Dong, X. Y., Du, J., Zhao, J. Y. & Zang, S. Q. MOF-Derived Bifunctional Cu3P Nanoparticles Coated by a N,P-Codoped Carbon Shell for Hydrogen

Evolution and Oxygen Reduction. *Adv. Mater.* **30,** 1–10 (2018).

92. He, P., Yu, X. Y. & Lou, X. W. D. Carbon-Incorporated Nickel–Cobalt Mixed Metal Phosphide Nanoboxes with Enhanced Electrocatalytic Activity for Oxygen Evolution. *Angew. Chemie - Int. Ed.* **56,** 3897–3900 (2017).

93. Zhao, S. *et al.* Ultrathin metal-organic framework nanosheets for electrocatalytic oxygen evolution. *Nat. Energy* **1,** 1–10 (2016).

94. Li, X. *et al.* ZIF-67-derived Co-NC@CoP-NC nanopolyhedra as an efficient bifunctional oxygen electrocatalyst. doi:10.1039/c6ta06434e

95. Jahan, M., Bao, Q. & Loh, K. P. Electrocatalytically active graphene-porphyrin MOF composite for oxygen reduction reaction. *J. Am. Chem. Soc.* **134,** 6707–6713 (2012).

96. Jiao, L., Zhou, Y.-X. & Jiang, H.-L. Metal–organic framework-based CoP/reduced graphene oxide: high-performance bifunctional electrocatalyst for overall water splitting. *Chem. Sci.* **7,** 1690–1695 (2016).

97. Yang, J. *et al.* Porous Molybdenum Phosphide Nano-Octahedrons Derived from Confined Phosphorization in UIO-66 for Efficient Hydrogen Evolution. *Angew. Chemie - Int. Ed.* **55,** 12854–12858 (2016).

98. Zhao, S. *et al.* Carbonized nanoscale metal-organic frameworks as high performance electrocatalyst for oxygen reduction reaction. *ACS Nano* **8,** 12660–12668 (2014).

99. Ai, L., Tian, T. & Jiang, J. Ultrathin Graphene Layers Encapsulating Nickel

Nanoparticles Derived Metal-Organic Frameworks for Highly Efficient Electrocatalytic Hydrogen and Oxygen Evolution Reactions. *ACS Sustain. Chem. Eng.* **5,** 4771–4777 (2017).

100. Xia, B. Y. *et al.* A metal-organic framework-derived bifunctional oxygen electrocatalyst. *Nat. Energy* **1,** 1–8 (2016).

101. Howarth, A. J. *et al.* Chemical, thermal and mechanical stabilities of metal-organic frameworks. *Nat. Rev. Mater.* **1,** 1–15 (2016).

102. Fang, Z., Bueken, B., De Vos, D. E. & Fischer, R. A. Defect-Engineered Metal-Organic Frameworks. *Angew. Chemie - Int. Ed.* **54,** 7234–7254 (2015).

103. Dou, S. *et al.* Atomic-Scale CoOx Species in Metal–Organic Frameworks for Oxygen Evolution Reaction. *Adv. Funct. Mater.* **27,** 1–8 (2017).